A LARGE *AGTR1* MISSENSE VARIANT LIBRARY FOR HIGH-THROUGHPUT PHARMACOGENOMIC SCREENING

Felipe de Jesus Navarro Vela

Principal Supervisor: Dr Joshua Dubowsky
Co-supervisor: Professor Harald Janovjak
Synthetic Physiology Laboratory

Thesis
Submitted to Flinders University
For the Degree of
Masters of Biotechnology

College of Medicine and Public Health
November 3rd, 2025

Table of Contents

Abstract

Hypertension is a chronic condition and the leading cause of morbidity and mortality worldwide, affecting over 400 million individuals around the globe. The angiotensin II type 1 receptor (AT_1R), encoded by the *AGTR1* gene, is a G protein-coupled receptor (GPCR) that plays a central role in regulating vascular constriction and salt-water homeostasis. Genetic variation in *AGTR1,* particularly missense mutations, can significantly alter receptor sensitivity to angiotensin II (AngII) and modify the intracellular signalling cascade contributing to hypertensive disease. Despite their potential clinical relevance, many naturally occurring *AGTR1* missense variants remain functionally uncharacterised, due to the small representation and study of population-specific variants within more representative medical research frameworks.

This research aimed to systematically characterise the functional diversity of *AGTR1* missense variants to better understand their impact on receptor activity and hypertension by building a comprehensive variant library. To achieve this, all reported missense substitutions were compiled from the gnomAD database and the scientific literature, yielding 406 unique targets for mutagenesis. A key innovation of this work lies in the establishment of a high-throughput, scalable site-directed mutagenesis (SDM) pipeline to generate an arrayed library of *AGTR1* variants, enabled by optimised primer design, *in vivo* two-fragment assembling, barcoding and long-read sequencing validation using next-generation sequencing. This approach achieved a 99.7% success rate in a single cloning round, demonstrating high accuracy and efficiency. The resulting arrayed *AGTR1* variant library covers over 400 validated constructs and represents the largest arrayed resource of its kind to date. Unlike pooled libraries, this arrayed format enables discrete analysis of individual variants, providing clear genotype-phenotype relationships and facilitating large-scale functional screening. Preliminary experiments established proof of concept for receptor activity in HEK293 cells, supporting the feasibility of implementing future high-throughput ligand-response screening. Given the association between *AGTR1* genetic variants and hypertensive treatment outcomes and risks, this work not only generated an unprecedented, high-quality *AGTR1* variant resource. It also introduced a highly economical and technically robust SDM workflow, broadly applicable to large-scale variant characterisation for improved understanding of variant-specific contributions to disease mechanisms and inter-individual variability in treatment response.

Declaration

I certify that this thesis:

1. Does not incorporate without acknowledgement any material previously submitted for a degree or diploma at any university
2. And the research within will not be submitted for any other future degree or diploma without the permission of Flinders University; and
3. To the best of my knowledge and belief, it does not contain any material previously published or written by another person except where due reference is made in the text.

Signed 

Felipe de Jesús Navarro Vela

Date: 03/11/2025

Acknowledgments

First and foremost, I would like to express my deepest gratitude to my supervisor, Dr Joshua G. Dubowsky, for their invaluable guidance, support and patience throughout this project. His insightful advice and encouragement were essential at every stage of my research. Together, we built this research project around a receptor and its disease-related aspects, which I have a personal interest in.

I would like to extend my sincere thanks to my co-supervisor, Professor Harald Janovjak, for the opportunity to be part of the Synthetic Physiology Group. I would also like to thank all my laboratory members for their collaboration, friendship, and positive atmosphere in the laboratory.

Most importantly, my heartfelt thanks go to my family: my mother, Lupita, my father, Daniel and my sister, Sandy. Their unwavering love, understanding and support have been the foundation of all my achievements; without them, I could not have come this far.

Para mi familia: No existen palabras suficientes para expresar con ellas toda la admiración y el amor que siento por ustedes (Daniel, Lupita y Sandy). Sé lo difícil que es no poder estar juntos en persona todo el tiempo; también mi corazón los extraña a cada paso. Este camino ha sido, a veces, duro y solitario, pero su cariño y su apoyo incondicional han sido la luz que me sostuvo cuando sentía que iba a rendirme.

Este logro no nace solo de mi esfuerzo, sino del nuestro. Cada avance, cada desvelo y cada duda superada llevan su nombre. Por eso, este reconocimiento no me pertenece únicamente a mí: también es suyo, porque juntos hemos andado este trecho en busca de mi sueño.

Cuando reciba mi reconocimiento por haber concluido mi maestría en biotecnología, se los entregaré en sus manos, como se ofrece una insignia a los verdaderos héroes de la historia. Será el reflejo del amor y la fuerza de la familia Navarro Vela.

Gracias por sostenerme en silencio, por creer en mí incluso cuando yo dudaba. Gracias por ser mi hogar, mi familia, aunque la distancia nos separe.

List of Figures

List of Tables

List of Abbreviations

Abbreviation	Full Form
7TMR	7 Transmembrane Receptor
°C	Celsius
µL	Microlitre
µM	Micromolar
AGTR1	Angiotensin II Type 1 Receptor Gene
AngII	Angiotensin II
AT_1R	Angiotensin II Type 1 Receptor
bp	Base pairs
CFU	Colony-Forming Unit
CV	Coefficient of Variation
CVD	Cardiovascular Disease
DMEM	Dulbecco's Modified Eagle Medium
DNA	Deoxyribonucleic acid
dNTPs	Deoxynucleotide triphosphates
DMSO	Dimethyl sulfoxide
E. coli	Escherichia Coli
FBS	Foetal Bovine Serum
g	Grams
GC	Guanine-Cytosine

Abbreviation	Full Form
GPCR	G Protein-Coupled Receptor
HBSS	Hank's Balanced Salt Solution
HHD	Hypertensive Heart Disease
kb	Kilobase
L	Litre
LA	Luria Agar
LB	Luria Broth
mA	Milliampere
mg	Milligrams
min	Minute
mL	Millilitre
mM	Millimolar
ng	Nanogram
nt	Nucleotide
ORF	Open Reading Frame
PCR	Polymerase Chain Reaction
PBS	Phosphate Buffered Saline
PLL	Poly-L-lysine
pg	Picogram
Q5	Q5 High-Fidelity DNA Polymerase

Abbreviation	Full Form
Q6U	Q6U High-Fidelity DNA Polymerase
RAS	Renin-Angiotensin System
rpm	Revolutions per minute
SDM	Site-Directed-Mutagenesis
SNP	Single Nucleotide Polymorphism
V	Volts
v/v	Volume/Volume
WT	Wild-Type
x g	Relative centrifugal force

Chapter I: Introduction

I.1 Clinical Impact and Therapeutic Challenges of Hypertension

Hypertension is a chronic condition and the leading global cause of death and disability, affecting more than 1.4 billion people worldwide in 2024 (World Health Organization., 2025). Uncontrolled blood pressure is a major contributor to cardiovascular disease (CVD), including stroke, chronic kidney disease, dementia and hypertensive heart disease (HHD). Between 1990 and 2019, global mortality from HHD reached 1.16 million, and it is projected to rise to 1.57 million by 2034 (Lu *et al.*, 2023). In Australia, diagnosing and treating hypertension costs $1.2 billion annually, with nearly 40% expenses paid by the patients. Most of these costs come from medication, pharmacy services, and general medical consultations, with blood pressure-lowering drugs alone accounting for approximately $100 million per year (Atkins *et al.*, 2024). Together, these overlooks underscore the significant health and economic burden posed by uncontrolled hypertension. Despite being preventable and treatable, global hypertension management continues to face numerous challenges globally, including low awareness, underdiagnosis, inadequate treatment adherence and limited access to validated blood pressure measurement devices in rural and low-income regions. For example, a review by Schutte *et al.* (2022) across the Asia-Pacific region in 2018 and 2019, only around 59% of individuals with hypertension are aware of their condition, 56% receive treatment, and less than one-third achieve effective BP control, highlighting ongoing deficiencies in detection and long-term management.

Current therapeutic strategies include both lifestyle modification and pharmacological interventions. Non-pharmacological management focuses on healthier dietary patterns, reduced sodium intake, increased physical activity, moderate alcohol consumption, and stress management (Verma *et al.*, 2021). Pharmacological therapy continues to be the central approach for moderating elevated BP and typically includes thiazide or thiazide-like agents, angiotensin receptor blockers (ARBs) and dihydropyridine calcium channel blockers (Al-Makki *et al.*, 2022; Seravalle & Grassi, 2023). Among these, ARBs are the most widely used to block the AT_1R receptor, the central regulator of vasoconstriction and sodium retention in the renin-angiotensin-aldosterone system (Seravalle & Grassi, 2023; Su *et al.*, 2021). Targeting AT_1R remains the first target for hypertension management and has driven research into underlying molecular mechanisms. Expanding on these therapies, precision or personalised medicine approaches consider each patient's unique factors, such as genes and environment,

using genomic, metabolomic, and proteomic analyses, artificial intelligence, and gene therapy to optimise treatment and mitigate variable drug responses (Dzau & Hodgkinson, 2024). Combining personalised medicine and pharmacogenomics-guided medication currently offers the best clinical outcomes compared to conventional approaches, aiming to tailor therapy based on individual genomic profiles and improve overall hypertension management (Hou *et al.*, 2024).

I.2 Structure, Function and Signalling of Angiotensin II Type 1 Receptor

The angiotensin II type 1 and type 2 receptors belong to the GPCR superfamily, and *AGTR1* is the principal gene receptor that mediates the majority of the hypertensive effects induced by AngII (Poudel *et al.*, 2023). The intracellular molecular signalling pathways activated by the AT_1R contribute to hypertension and CVD by promoting oxidative stress, hypertrophic remodelling and inflammation (Kawai *et al.*, 2017). GPCRs share a conserved seven-transmembrane receptor (7TMR) domain structure with an extracellular-facing ligand binding site and an intracellular pocket for transducer binding (Liu *et al.*, 2024).

As shown in the simplified diagram in Figure 1, the AT_1R receptor primarily mediates its effects by coupling to the Gq/11 subunit of the Gα heterotrimeric G protein family (Hubbard & Hepler, 2006; Liu *et al.*, 2024; Simon *et al.*, 1991; Zaman *et al.*, 2002). Receptor activation happens when angII binding occurs within the ligand-binding pocket formed by transmembrane helices 3, 5, 6 and 7. Ligand binding induces conformational changes in the GPCR transmembrane helices propagated by intracellular loops (ICL2 and ICL3) (Heng *et al.*, 2023). This conformational rearrangement permits the receptor to act as a guanine nucleotide exchange factor (GEF) for the Gα subunit, promoting the exchange of guanosine triphosphate (GTP) for guanosine diphosphate (GDP) (Gilman, 1987; Goodfriend *et al.*, 1996; Liu *et al.*, 2024; Tsunoda *et al.*, 1997; Zaman *et al.*, 2002). This induces dissociation of the Gα-GTP subunit from the $G_{\beta\gamma}$ complex, allowing each of these units (Gα, Gβ and Gɣ) to interact with a wide range of effectors independently (Liu *et al.*, 2024). We are interested in on one family of the sixteen Gα subunits, specifically the $G\alpha_q$/11, which activates phospholipase-Cβ (PLCβ), and hydrolyses membrane phosphatidylinositol 4,5-biphosphate (PIP2) into two second messengers: diacylglycerol (DAG) and inositol 1,4,5-triphosphate (IP3) (Liu *et al.*, 2024). IP3 binds to cardiomyocyte IP3 receptors located on the sarcoplasmic reticulum and nuclear envelope, stimulating a release of Ca2+ (Liu *et al.*, 2024). This Ca2+ release is distinct from the cytoplasmic Ca2+ transients responsible for excitation-contraction coupling, which activate

hypertrophic signalling pathways through calcium-dependent effectors such as calcineurin and Ca^{2+}/calmodulin-dependent protein kinase II (Liu *et al.*, 2024), an event which promotes cellular hypertrophy.

At the same time, DAG and the rise in intracellular Ca2+ activate protein kinase C-alpha (PKC-α), which influences cardiac contractility by upregulating type 1 protein phosphatase. This enzyme dephosphorylates phospholamban, a regulator of the sarcoplasmic reticulum Ca2+ ATPase pump, thereby modulating sarcoplasmic reticulum Ca2+ uptake and impacting muscle relaxation and contractile force (Gilman, 1987; Liu *et al.*, 2024; Pierce *et al.*, 2002; Sprang *et al.*, 2007).

Following sustained activation, *AGTR1* becomes phosphorylated by rhodopsin kinase, also known as G protein-coupled receptor kinases (GRKs) on its C-terminal tail (Lefkowitz & Shenoy, 2005; Oakley *et al.*, 2000). This phosphorylation enables the β-arrestin complex to bind to the activated receptor, internalising both the receptor and the β-arrestin complex into the cell. At this stage, both remain in endosomal vesicles for a time before being redirected to lysosomes or slowly recycled (Lefkowitz & Shenoy, 2005). This process plays a crucial role in receptor re-sensitisation, receptor recycling, receptor down-regulation and receptor signalling (Lefkowitz & Shenoy, 2005).

These mechanisms illustrate how $G\alpha_q$/11-mediated signalling coordinates calcium dynamics and kinase/phosphatase activities to regulate both cardiac muscle contraction and hypertrophic growth responses, key processes in cardiac physiology and disease.

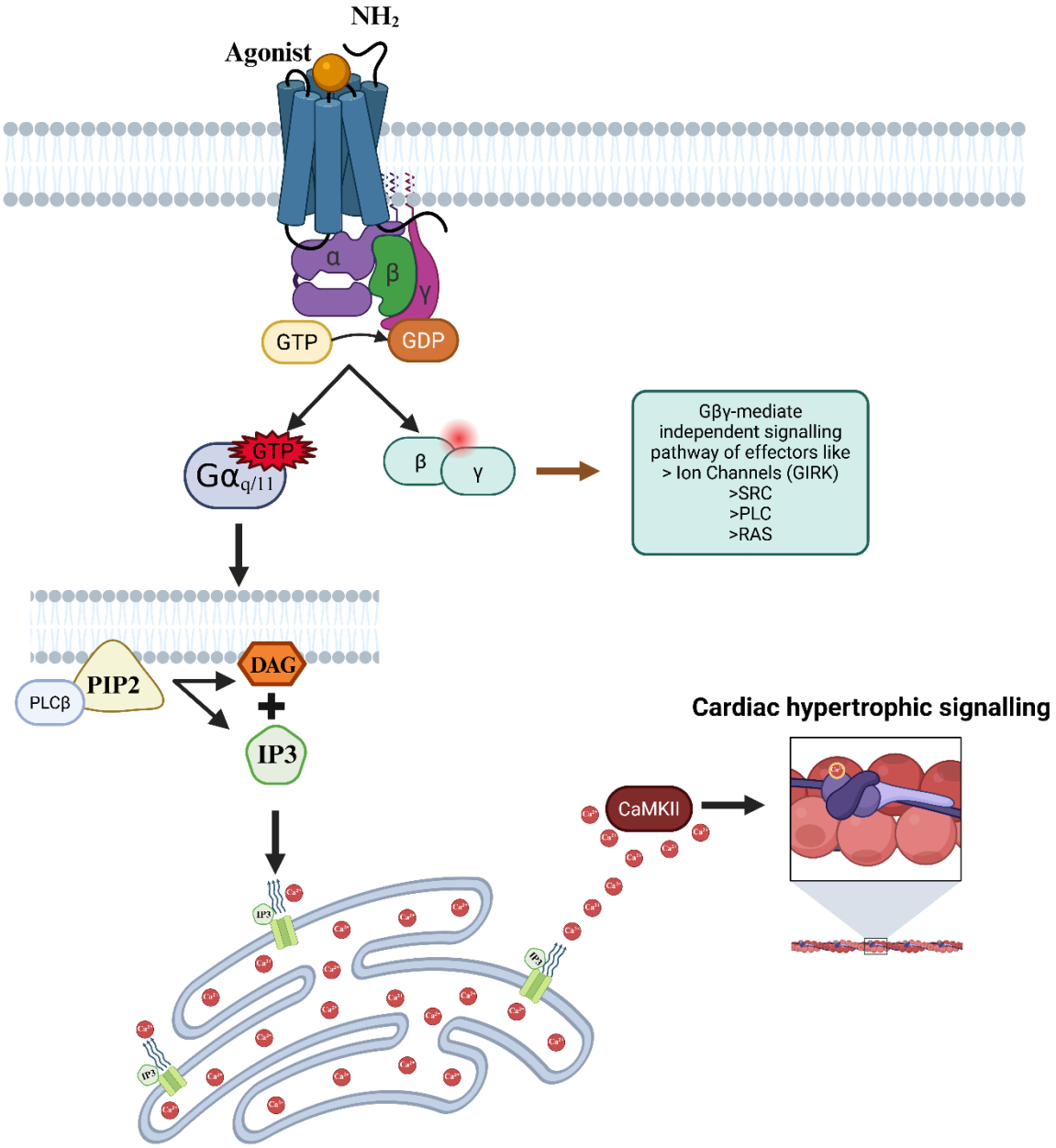

Figure 1 | **Gαq/11-Mediated AT_1R Signalling Pathway in Hypertension.**

Angiotensin II type 1 receptor signalling through the Gαq/11 heterotrimeric G-protein. Angiotensinogen by renin and angiotensin-converting enzyme to yield the peptide AngII. Agonist binding to AT_1R, the receptor undergoes a conformational change allowing Gα dissociation and Gαq/11 activation via GDP-GTP exchange. Activated Gαq stimulates PLCβ. Generating IP3 and DAG. IP3 binds to the IP3-receptor and releases calcium from the sarcoplasmic reticulum and nuclear envelope, activating cardiac hypertrophic signalling via CaMKII. Created in https://BioRender.com.

I.3 Genetic Variability and Pharmacogenomic Implications of *AGTR1*

Single-nucleotide polymorphisms (SNPs) represent the most common form of human genetic variation. When it is located within the coding region, these changes can alter the resulting amino acid sequence, consequently affecting protein folding, structural stability, intermolecular interactions and post-translational modifications (Israr *et al.*, 2025). Such variants contribute greatly to differences in protein function and disease susceptibility. Within the renin-angiotensin system (RAS), several genes play a crucial role in regulating the cardiovascular system. Among these, *AGTR1* encodes the AT_1R receptor, a 359 amino acid GPCR (Mauzy *et al.*, 1992; Ziaja *et al.*, 2021). Variants in *AGTR1* can influence receptor expression and signal transduction efficiency, contributing to the pathogenesis of hypertension, CVD and renal disorders (Agostini *et al.*, 2024; Grimson *et al.*, 2016).

Specific missense substitutions within *AGTR1* gene have been shown to have a significant impact on receptor function. These genetic variants can modify AT_1R conformational dynamics, G-protein coupling and β-arrestin recruitment, which ultimately affect downstream signalling and therapeutic responses (Mahoney & Sunahara, 2016; Oro *et al.*, 2007; Zhu *et al.*, 2019). One residue of particular interest is asparagine at position 111 ($N111^{3.35}$) located in the third transmembrane domain. This amino acid plays a crucial role in making the receptors inactive conformation by maintaining a hydrogen-bonding network essential for efficient signal transmission from the ligand-binding pocket to the intracellular Gq/11 and β-arrestin pathways (Auger-Messier *et al.*, 2003; Zhang *et al.*, 2023). Mutational studies have demonstrated that substitutions at $N111^{3.35}$ alter receptor activity. Specific changes like N111A, N111G, and N111S are known to induce constitutive activation of AT_1R, while N111W results in loss of function. (Auger-Messier *et al.*, 2003; Billet *et al.*, 2007; Zhang *et al.*, 2023). Among constitutively active mutations, the N111S mutation is notable for causing constitutive internalisation, resulting in intracellular sequestration of most receptor molecules (Billet *et al.*, 2007). Highlighting the relevance in pharmacogenomics of this location variant of *AGTR1* and its impact on treatment outcomes.

I.4 Site-Directed Mutagenesis (SDM)

Site-directed mutagenesis is a cornerstone technique in molecular biotechnology, widely used to characterise gene and protein structure, study protein-protein interactions and define protein-binding domains (Carrigan *et al.*, 2011). SDM employs synthetic oligonucleotides designed to be complementary to a specific DNA sequence but containing intentional mismatches to introduce the precise mutation. These mutations can include base substitutions, insertions and deletions within the double-stranded plasmid DNA, allowing for targeted alterations at the nucleotide level (Iqbal & Sadaf, 2022).

Historically, mutagenesis began with non-specific methods such as X-ray irradiation in 1972, which induced random genomic mutations and required extensive screening (Alberts *et al.*, 2002; Zheng *et al.*, 2017). The field advanced significantly in the early 1980s with the oligonucleotide-directed mutagenesis (ODM), which utilises single-stranded bacterial vectors and synthetic oligonucleotides to create highly specific mutations, laying the foundation for modern SDM techniques (Gocal *et al.*, 2015; Moerschell *et al.*, 1988). The introduction of PCR in 1985, and its three major phases (denaturation, annealing and extension of DNA) further revolutionised mutagenesis by enabling amplification of mutated DNA sequences. Coupled with thermostable DNA polymerases, PCR-based SDM became highly efficient and reproducible (Khehra *et al.*, 2025).

Despite these technological advances, traditional SDM methods face limitations when applied to large-scale variant libraries due to high costs, labour-intensive workflows and limited scalability. These bottlenecks hinder comprehensive screening efforts, such as in the case of the *AGTR1* missense variant library central to this project. To overcome these challenges, this project employs a high-throughput, arrayed mutagenesis pipeline that enables systematic generation of hundreds of receptor variants simultaneously. This strategy uses optimised primer design to enhance specificity and efficiency, parallel cloning techniques to process multiple variants in tandem, and the use of high-fidelity polymerases to ensure accurate amplification. Together, these elements enable rapid, cost-effective synthesis of a large-scale variant library directly compatible with functional cell-based assays, significantly improving scalability and throughput compared to conventional SDM methods.

I.5 Current Functional Screening, Its Application and Limitations

Functional screening of *AGTR1* variants is crucial to understand how genetic differences impact receptor function, drug response and the hypertension mechanism (Hansen *et al.*, 2004). Advances in genomics have identified several *AGTR1* missense variants, creating a need for efficient methods to assess their functional impact on a large scale. Functional screening generally falls into three categories: *in silico* prediction, pooled high-throughput assays and well-by-well high-throughput assays (Yasi *et al.*, 2020).

In silico prediction methods utilise computational methods such as SIFT, PolyPhen-2, MUpro, I-Mutant 3.0, MutPred2 or Chimaera to estimate the effects of variants on protein stability, function, post-translational modifications, and interactions (Israr *et al.*, 2025). However, their application in GPCR studies like *AGTR1* is limited by challenges in accurately modelling GPCRs complex conformational dynamics, often relying on unreliable templates from distant homologs (Shacham *et al.*, 2004). Consequently, *in silico* predictions may miss minor but functionally important effects on receptor activation, ligand binding, and G-protein coupling. This limitation underscores the critical need for experimental validation.

Pooled high-throughput assays, such as multiplexed assays of variant effects, enable functional testing of hundreds of variants at the same time by introducing mutations through homology-directed repair. However, these methods are limited to editing small genomic regions, working on small regions from 100-200 bp per experiment, necessitating multiple libraries to cover the complete *AGTR1* coding sequence (Herger *et al.*, 2025). Additional challenges include variable editing efficiency, incomplete substitution coverage, and scalability concerns (Glazer *et al.*, 2025). Therefore, pooled assays require complementary targeted approaches to confirm results.

Arrayed high-throughput screening involves testing each variant individually in separate wells (Valentine & Tigyi, 2012), enabling detailed dose-response curves, direct drug interaction testing and the reduction of technical noise from barcodes. This format is well-suited to clinical validation and integration of multiple (Mahjour *et al.*, 2023; Zeghal *et al.*, 2023). Although the traditionally arrayed method has its limitations, such as scalability, labour-intensive and cost (Valentine & Tigyi, 2012; Yin *et al.*, 2025). Such limitations can be improved with automation.

This study builds upon a pre-existing *AGTR1* plasmid developed by Rahkesh T. Sabapathy and employs an arrayed high-throughput approach using 96-well assays and parallel processing to rapidly and systematically characterise over 400 missense variants within six months. This workflow provides a cost-effective, scalable platform for pharmacogenomic investigation of *AGTR1* variants.

I.6 Hypothesis and Aims

Hypothesis: Due to variable *AGTR1* genotypes in the population, the global population possesses *AGTR1* mutants that will respond differently to AngII. Comprehensive functional screening of a large *AGTR1* missense variant library will identify variants that alter receptor activity.

Aims:

1. To compile and curate a comprehensive *AGTR1* missense variant list from the gnomAD database and relevant literature.
2. To generate a large-scale library of *AGTR1* mutant constructs using an in-house, high-throughput cloning pipeline.
3. To develop and validate an assay in *AGTR1*-transfected HEK293 cells that measures ligand-induced functional responses. Focusing on differences in receptor signalling behaviour upon stimulation with AngII.

Chapter II: Materials and Methods

II.1 Liquid Luria Broth Media (Miller) Protocol

Luria Broth (Miller) medium was prepared by dissolving Luria Broth Powder (HIMEDIA, GM1725), at 15.52 g/L, supplemented with sodium chloride 95mM (Sigma, S9888) and magnesium chloride (Sigma, M8266) 0.4mM in Milli-Q water. The solution was sterilised by autoclaving at 120 ℃ for 20 minutes. After cooling to approximately 50 ℃, a 1:1000 dilution of 1000X ampicillin stock solution was supplemented.

II.2 Luria Agar (granulated) Protocol

LA (Luria Agar, granulated) medium was prepared by dissolving LA powder (HIMEDIA, GM557) to a final concentration of 35 g/L in Milli-Q water. The mixture was sterilised by autoclaving at 120 ℃ for 20 minutes. Following sterilisation. After cooling to approximately 50 ℃, add a 1:1000 dilution of 1000X ampicillin stock solution.

II.3 Removal of the mCherry Fluorescent Fusion Protein from the *AGTR1* Plasmid

To remove the mCherry fluorescent fusion protein, site-directed mutagenesis PCR (SDM) was performed using primers OJ107/SDM1R and OJ108/SDM1F. The SDM1R and SDM1F are specially designed primers to anneal to the ampicillin resistance sequence in the plasmid backbone. Primers were designed to include the *AGTR1* coding sequence while introducing a new stop codon to exclude the mCherry fusion. Primer melting temperatures were predicted using laboratory software tools to confirm compatibility with the PCR cycles and temperatures. The thermocycler steps and primer sequences are in Table 1 and Table 2, respectively. PCR set up for Q5 PCR protocol includes Milli-Q water, Q5 Reaction Buffer (NEB, B9027S), DNA (500 pg/µL), PBJ universal forward primer (10 µM), specific reverse primer for each batch (10 µM), Q5 High GC Enhancer (NEB, B9028A), dNTPs (Betoyime, D76DZ), and Q5 High-Fidelity DNA Polymerase (NEB, M0491L) in a final volume of 25 µL.

Resulting amplicons were treated with DpnI for DNA template removal, subsequently, both fragments were mixed stoichiometrically for two-fragment *in vivo* assembling using competent cells XL-10 *E. coli.*

II.4 Primer Design

Primers for SDM were designed to introduce a library of 406 *AGTR1* missense mutations across the entire coding sequence. For each mutation, the full *AGTR1* ORF(all 359 amino acids) was submitted as a FASTA sequence to NEBaseChanger online tool (https://nebasechanger.neb.com/), site-specific substitutions were specified using the nucleotide position and desired change. The minimum primer length parameter was set to 20 nt, and the minimum primer time (TM) was set at 70 ℃. The reverse complements of the primers were generated using an in-lab Excel worksheet. All primers were synthesised by Integrated DNA Technologies and received as lyophilised powder. Upon receipt, the oligonucleotides were resuspended in Mili-Q water to a stock concentration of 5 µM and stored at -20 ℃.

II.5 Site-Directed Mutagenesis PCR

Site-directed mutagenesis PCR (SDM-PCR) was performed using oligonucleotide primer pairs designed for specific *AGTR1* mutations. For high-throughput processing, separate master mixes were prepared and dispensed into a 96-well semi-skirted PCR plate (BIO-RAD, HSS9601), assigning one primer pair in each well to generate distinct variants. The PCR set-up followed the laboratory Q6U PCR planner workflow.

Reagents used for Q6U PCR protocol were Milli-Q water, 10X Q6U Buffer (Betoyime, D7239L-2), template DNA (500 pg/µL), a pair of mutagenic primers (one carrying the nucleotide substitution and its complementary counterpart annealing to the opposite strand), dNTPs (Betoyime, D7366) and Q6U High-Fidelity polymerase (Betoyime, D7239L-1) in a final volume of 25 µL. PCR parameters are listed in Table 3.

II.6 Agarose Gel Electrophoresis Protocol

A 1% agarose gel was prepared by dissolving half of a SeeGreen All-in-One Agarose Tab (miniPCR, RG-1500-20) in Milli-Q water and heating in a microwave until fully dissolved, avoiding overboiling. After cooling and solidification, the gel was placed in a blueGel electrophoresis chamber containing 1X TBE buffer (Sigma, T4415). DNA samples were prepared by combining one part of the DNA sample, five parts loading dye, and nineteen parts of Milli-Q water. A 1 kb Plus DNA ladder (NEB, N3232) was loaded in the first well as a

molecular size marker. Electrophoresis was performed at 90 V and 120 mA for 20 – 30 minutes, and the DNA fragments were visualised using the integrated transilluminator of the gel system.

II.7 Tow-Fragment Assembly by *E. coli In vivo* Recombination

Equimolar amounts of the forward and reverse PCR amplicons generated by SDM PCR were mixed to a total volume of 10 µL. To remove residual template plasmid DNA, 1 µL of DpnI restriction enzyme (NEB, R0176L) was added, and the reaction was incubated at 37 ℃ for 90 minutes. 1.6 µL of the DpnI-digested product was transformed into 20 µL of XL10-Gold Ultracompetent *E. coli* cells (NEB, C3040), followed by incubation on ice for 20 minutes. Transformed cells were plated on LA medium supplemented with ampicillin (100 µg/mL) and incubated overnight at 37 ℃.

II.8 Colony Selection and Plasmid Mutant Screening

Each mutant variant was plated on Luria agar medium supplemented with ampicillin (100 µg/mL) in trays pre-divided into compartments arranged in a 6 x 8 grid, allowing simultaneous processing of multiple colonies. Three individual colonies were randomly selected and inoculated into separate 96-well round-bottom plates (Costar, 3788) containing 200 µL of LB medium supplemented with ampicillin (100 µg/mL) and sealed with sterile breathable sealing film (Adelab Scientific, BF-400-S). Cultures were incubated at 37 ℃ with shaking at 600 rpm for 10 hours.

II.9 Plasmid DNA extraction and purification

Selected colony for subsequent downstream analysis and experiments, plasmid DNA was extracted and purified by using SanPrep Column Plasmid Mini-Preps Kit (Sangon Biotech, B518191-0100). 2 mL of overnight bacterial culture was harvested and centrifuged at 10,000 x g for 2 minutes. The supernatant was discarded, and the bacterial pellet resuspended in 250 µL of buffer P1 (B900001-1000) supplemented with RNase (B900068-0001) by performing 5 passes on the rack. Subsequently, 250 µL of buffer P2 (B900002-1000) was added, and the tube was inverted 10 times to mix, followed by a 2 minutes incubation at room temperature for cell lysis. Then, 350 µL of buffer P3 (B900003-1000) was added, mixed by inversion 10 times, and centrifuged at 12,000 x g for 10 minutes to pellet cellular debris. The clarified supernatant was transferred to the SanPrep spin column and centrifuged at 10,000 x g for 30 seconds, the flow-through was discarded. The column was washed with 500 µL of buffer DW1 (B900005-1000)

by centrifugation at 10,000 x g for 30 seconds; the flow-through was discarded. Two washes were performed with 500 µL of wash solution (B900009-1000) supplemented with 96 µL of 100 % ethanol, each followed by centrifugation at 10,000 x g for 30 seconds and discarding the flow-through. To eliminate residual wash buffer, the column was centrifuged at 10,000 x g for 2 minutes. Finally, plasmid DNA was eluted by adding 40 µL of Elution buffer (B900012-1000) to the column membrane, incubating for 1 minute at room temperature, and centrifuging at 10,000 x g for 60 seconds. The purified plasmid DNA was stored at -20 ℃ for subsequent use.

II.10 Working Culture Collection and Glycerol Stocks

From each 96-well plate, a working culture was separated to continue with the experiment and a 20 µL volume was removed and pooled into a 2 mL tube. Following working culture separation, for long-term preservation and to prevent the formation of ice crystals that can damage the bacteria during freezing, 75 µL of 16 % v/v glycerol was added to each well and stored at -80 ℃.

II.11 Plasmid DNA Preparation

Each 2 mL pooled working culture was centrifuged at 12,000 rpm for 2 minutes using a Fresco 17 microcentrifuge (Thermo Fisher Scientific, THR75002420). Plasmid DNA was extracted using SanPrep Column Plasmid Mini-Preps Kit (Sangon Biotech, B518191-0100). After DNA extraction, the DNA concentration and purity were assessed by spectrophotometer using a Nanodrop 2000C Spectrophotometer (Thermo Fisher Scientific, ND-2000).

II.12 PCR Barcoding and Library Pooling

Every mutant set plate from the three batches was processed separately with its own master mix and assigned a specific reverse primer, along with a universal forward primer. For each batch of mutant set plates, a separate PCR master mix was prepared with the following components: Milli-Q water, Plasmid DNA (500 pg/µL), Q5 Reaction Buffer (NEB, B9027S), dNTPs (Betoyime, D76DZ), Q5 High GC Enhancer (NEB, B9028A), Q5 High-Fidelity DNA Polymerase (NEB, M0491L), universal forward primer (PacBio 16S_Fwd_12) at 10 µM, and barcoded reverse primers for each batch; PacBio 16S_Rev_42, PacBio 16S-Rev_43 and PacBio 16S_Rev_44 (primers sequences are found in Table 4) all at 10 µM. Each reaction was assembled in a final volume of 25 µL using 5 ng/µL diluted plasmid DNA as template.

Barcoded PCR reactions were set up according to the laboratory Q5 PCR planner workflow (detailed in Table 5). Following PCR amplification using the respective cycling parameters (Table 6). Amplicons generated using each barcoded reverse primer were separately pooled per batch, resulting in three distinct tubes, one for each barcoding sequence.

II.13 AMPure DNA Purification

The purification mixture was prepared by combining pooled PCR amplicons from each batch with silica-coated superparamagnetic beads (Cytiva, 29357369) premixed with 70 % ethanol, into a 1.5 mL DNA Lobind tube (Eppendorf, 0030108418) in a bead-to-sample volume ratio of 0.8 and 27 µL of Milli-Q water. The mixture was thoroughly mixed and spun down for 1 second. DNA binding was performed by incubating the mixture for 10 minutes at room temperature on a vortex mixer (JOANLAB, VM503) set at 2000 rpm. After incubation, the tube was spun down again for 1 second. The tube was then placed in a magnetic bead rack until the beads collected on the side for 2 to 5 minutes at room temperature until the solution became clear. With the tube still in the magnetic bead rack, pipette off the cleared supernatant without disturbing the bead pellet. The beads were washed twice with 750 µL of freshly prepared 70 % ethanol and avoiding disturbing the bed pellet. After washing, the tube was left to air dry with the tube cap opened for 60 seconds. For elution, 40 µL of 25 mM Tris-HCL (pH 8.0) was added to the beads, and the tube was vortexed for 2 minutes at 2000 rpm. The pellet was then spun down for 1 second and placed in a magnetic bead rack, and the elution was collected, discarding the beads.

II.14 Library Sequencing

Genomic DNA libraries were sequenced by Gnomix Pty Ltd. using an Oxford Nanopore PromethION 2 Solo with FLO-PRO114M flow cells and SQK-NBD114-24 kit. Run setting to 1 hour and 46 minutes. FASTQ data were generated every 10 minutes, and all reads with a Q score below 10 were discarded. A total of 1,450,000 reads were produced with a read length N50 of 1.51 kb. The quality scores of passing reads peaked around Q20-23. Read quality remained stable throughout the run.

II.15 HEK293 Cell Preparation and Maintenance

HEK293 cells, which were obtained from a previous actively proliferating culture (a kind gift from Professor Luke Selth), were maintained under standard mammalian cell culture

conditions in Dulbecco's Modified Eagle Medium (DMEM; Gibco™, 11995-065). Routine passages were performed twice weekly under aseptic conditions in a class II Biosafety Cabinet (51034895, Thermo-Scientific).

Cell passage begins by removing the culture medium, followed by washing the adherent cells once with Phosphate Buffered Saline (PBS), (-) Calcium Chloride, (-) Magnesium Chloride at pH 7.2 (Gibco™, 20012-027), After aspirating the PBS, 2.5 mL of 0.05 % Trypsin-EDTA (Gibco™, 25300-054) is added to the flask which is then incubated at 37 ℃ for 1 minute to detach the cells. The reaction is halted by adding 5 mL of pre-warmed Dulbecco's Modified Eagle Medium (DMEM), (+) 4.5g/L D-glucose, (+) L-Glutamine and 110mg/L Sodium Pyruvate (Gibco™, 11995-065), supplemented with 5 % Foetal Bovine Serum (FBS) (Gibco™, A56709-01). An aliquot of 10 µL of the cell suspension is mixed with an equal volume of Trypan Blue Stain 0.4 % (Gibco™, 15250-061), and 10 µL of this mixture is loaded onto a LUNA™ Reusable Slide (Logos biosystems, L12011). Cell confluency is determined using the LUNA-FL™ Dual Fluorescence Cell Counter (Logos biosystems, L20001). Based on the cell count, the cells are diluted to a concentration of 3.5 X 10^5 cells per mL and seeded into a new T75 flask (corning®, 430641U) containing 17 mL of DMEM. The flask is incubated at 37 ℃ in a humidified atmosphere of 5 % CO_2 atmosphere until the next passage.

II.16 Poly-L-lysine Plate (PLL) Coating

Coating was performed under a class II Biosafety Cabinet. From a sterile Poly-L-lysine solution 0.1 % (w/v) in H_2O (Sigma-Aldrich, 25988-63-0), a 1:89 dilution using PBS was performed, covered with 200 µL of the PLL dilution in each well of the black-walled, clear-bottom 96-well tissue culture-treated polystyrene assay plates (COSTAR®, 3603) with lid on and incubated at room temperature for 1 hour. After the incubation time, PLL was aspirated from the wells and washed three times with sterile Water for Irrigation (Baxter, AHF7114) and left air-dry with the lid off for 1-3 hours. The coated plate is stored at 4 ℃ until use.

II.17 HEK293 Plate Seeding

HEK293 cells were seeded in a Poly-L-lysine-coated 96-well plate at a density of 30,000 cells per well. Cells were prepared from a suspension at 3 x 10^5 cells/mL in a total volume of 10 mL,

with 100 µL of this suspension seeded into each well. Incubate the seeded plate at 37 ℃ in a humidified 5 % CO_2 atmosphere for 24 hours.

II.18 HEK293 Cell Transfection with *AGTR1* plasmid

HEK293 cells at 70-90 % confluency were transfected using FuGene® HD Transfection Reagent (Promega, E2311), following manufacturer instructions with modifications to optimise transfection efficiency for *AGTR1* constructs. For each well, 100 ng of *AGTR1* plasmid DNA was complexed with FuGene® HD at a 1:6 DNA-to-reagent ratio, then adjusted to a final volume of 10 µL with Opti-MEM (Gibco™, 31985070) and incubated for 15 minutes at room temperature before addition to cells. Fresh growth medium was provided immediately prior to transfection. Reaction volumes were scaled proportionally to the number of wells, and the plates were incubated for 48 hours under standard mammalian cell culture conditions.

II.19 Calcium Assay Validation

HEK293 cells seeded in black-walled, clear-bottom 96-well plates were loaded with 4 µM Fluo-4 AM (ABP Biosciences, C219) diluted in Hanks' Balanced Salt Solution (HBSS, Sigma-Aldrich, H6648-500ML) without phenol red, calcium chloride and magnesium sulfate. After 48 hours of transfection, the culture medium was removed and 100 µL of Fluo-4 AM solution was added to each well. The plates were incubated in the dark for 30 minutes at 37 ℃. The microplate reader (CLARIOstar Plus, BMG LABTECH, 430-4001) was prewarmed to 37 ℃. AngII human stock (1000 µM, MedChemExpress, HY-13948) was prepared by dissolving the peptide in Dimethyl sulfoxide (DMSO, MedChemExpress, HY-Y0320) and serially diluted for dose-response assessment. Following incubation with the dye, the Fluo-4 AM solution was removed, and the cells were washed twice with HBSS. Calcium assay tested different conditions such as well volumes of HBSS (100, 200 and 300 µL), injection volumes (1, 5, 10 and 15 µL) and injection speeds (50 µL/s and 430 µL/s) to optimise assay conditions. Fluorescence signals were recorded using excitation at 483 nm and emission at 530 nm with bottom optic detection mode. Readings were taken at 1 second intervals over 100 seconds' period. Following a 10 second baseline acquisition, ligand or buffer was injected, and orbital shaking at 100 rpm was applied immediately after injection.

II.20 Data Analysis

Fluorescence signals were normalised to the injection fluorescence as baseline and the maximum value as the higher value across the experiment, using a min-max scaling approach. Comparative analyses assessed the effects of experimental variables and the *AGTR1*_WT. Normalised fluorescence was used to evaluate assay consistency and reproducibility. The coefficient of variation (CV) was calculated for the negative control to quantify signal variability and determine if the observed noise fell within an acceptable range. Key parameters such as fluorescence intensity, time to maximum fluorescence (Tmax), maximum-baseline values and delta max (Δmax), quantified the response and kinetics. Scatter plots of normalised runs, which were generated to visualise data distribution and assess reproducibility. Statistical comparison between *AGTR1* and experimental conditions was performed to identify significant differences, while dose-response curves were used as a reference to characterise receptor activity changes. The analytical approach was tailored to support the functional evaluation of *AGTR1* variants generated through high-throughput.

Chapter III: Results

III.1 Removal of mCherry Tag from *AGTR1* Plasmid

A pre-existing *AGTR1*_mCherry plasmid constructed in the laboratory by Mr Rahkesh T. Sabapathy, served as the template construct for this project. The objective was to remove the mCherry fusion protein from the plasmid. To achieve this, PCR was used to exclude the mCherry coding sequence. Two overlapping linear DNA fragments that cover the entire plasmid were generated in two separate reactions, one for each strand. The overlapping ends were designed to be homologous and is known to play an important role in balancing the colony number proliferation, while also maintaining a high assembly accuracy (Huang *et al.*, 2017). This overlapping strand represents an optimal balance between assembly efficiency, cost, and nonspecific priming risk.

The resulting DNA fragments, each containing between 25-30 bp overlapping nucleotides and homologous ends, were assembled into XL-10 *E. coli* competent cells. Endogenous homologous recombination within *E. coli* permits the reassembly of the entire circular plasmid without the need for ligation or restriction enzymes. This two-fragment assembly approach provides a rapid and accurate way of plasmid reconstruction.

PCR amplification using specific primer pairs targeting the 5' and 3' regions of *AGTR1* produced two strands with predicted sizes of 2,388 bp and 2,270 bp. The presence and expected lengths of the amplicons were confirmed by agarose gel electrophoresis (Figure 2). Following bacterial transformation, three individual transformed *E. coli* colonies were selected for plasmid extraction using the SanPrep Column Plasmid Mini-Preps Kit. Purified plasmid DNA was quantified spectrophotometrically, and the sample with the highest concentration and optimal purity was selected for further verification.

The isolated plasmid was subjected to restriction enzyme digestion with HindIII, which cuts at two distinct sites common to both *AGTR1*_mCherry and the modified *AGTR1* plasmid. Analysis of the digested products by agarose gel electrophoresis confirmed each fragment size which resulting in a plasmid size corresponding to a plasmid with no mCherry protein sequence (Figure 2). To evaluate sequence integrity, the reconstructed plasmid was subsequently sequenced using Oxford Nanopore long-read sequencing. Sequence comparison using EMBOSS Needle Pairwise Alignment (https://www.ebi.ac.uk/jdispatcher/psa/emboss_needle) showed that the *AGTR1* coding sequence in the constructed plasmid was identical to that in the

original plasmid by Rahkesh T. Sabapathy construct and corresponds to the canonical human *AGTR1* entry reported in UniProt (Entry: P30556). However, three additional nucleotides were detected in the reconstructed plasmid outside the *AGTR1* coding region. This validation ensured that the plasmid used for subsequent experimental work in this project was based on the biologically authentic AT1R receptor.

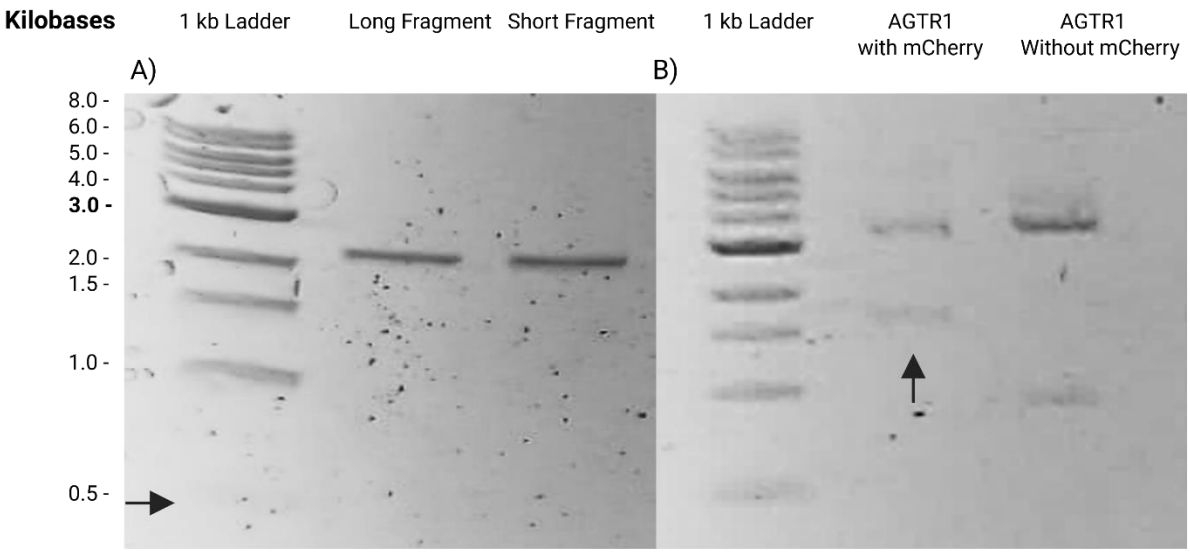

Figure 2 | **Agarose gel profiles of PCR and HindIII-digested *AGTR1* plasmids.**

(A) Agarose gel electrophoresis showing PCR amplicons corresponding to the two overlapping DNA fragments generated for *AGTR1* plasmid reconstruction. The observed band sizes were consistent with the predicted lengths of the long and short amplicons from the plasmid assembly. (B) HindIII restriction digestion of *AGTR1* plasmids with and without the mCherry protein sequence produced two distinct DNA fragments of different sizes, consistent with successful modification of the plasmid construct. A 1 kb DNA ladder was included as a molecular size reference for both gels. The black arrow indicates a faint band that was difficult to visualise under standard exposure conditions. Created in https://BioRender.com

III.2 Comprehensive Coverage of *AGTR1* Missense Variants

A comprehensive list of *AGTR1* missense variants was compiled by extracting population genetic data from the gnomAD database, which aggregates a large-scale exome and genome sequencing data from over 800,000 individuals worldwide (Katherine Chao, 2023). Additional variants with reported effects on Ang II binding or responsiveness to ARBs were curated from peer-reviewed scientific literature. Each variant was annotated with its allele frequency to assess global representation. Based on the total summed allele frequency of $8.27x10^{-3}$ for the compiled variant list, the library was estimated to represent approximately 1.65% of the global population, equivalent to around 135 million individuals as of 2025. This coverage underscores the relevance of the *AGTR1* variant library for investigating population-level receptor diversity and pharmacogenomic variation (Figure 3).

To assess the potential functional impact of each variant of the *AGTR1* missense library, AlphaMissense (https://alphamissense.hegelab.org/results), a computational tool, was used to predict variant pathogenicity. This computational framework scores all possible amino acid substitutions across the human proteome from 0 to 1, classifying them as likely benign (≤0.344), ambiguous (0.345-0.564), and likely pathogenic (≥0.565) (Krenn *et al.*, 2025). Each *AGTR1* variant in our library was annotated with it corresponding AlphaMissense score to provide a comprehensive functional profile. AlphaMissense scoring of the variant library revealed that the majority of the mutants are predicted to be pathogenic. Out of the 405 successfully generated mutants, 54 were classified as likely benign, 17 as ambiguous and 334 as likely pathogenic. Stratifying the data by category (Figure 4), demonstrates the full range of potential functional consequences encoded within the library. Most likely benign variants suggest minimal impact on receptor function, while likely pathogenic variants are more frequent in those variants located outside the transmembrane domain, denoting highly conserved residues that are predicted to have a severe disruption. The predominance of predicted pathogenic variants among those identified in gnomAD highlights the potential functional importance of naturally occurring *AGTR1* mutations and reinforces the value of this variant library for experimental pharmacological assessment.

Primers for *AGTR1* SDM were designed using the NEBaseChanger online tool (https://nebasechanger.neb.com/), resulting in 840 unique oligonucleotides targeting individual missense variants. Using these primers, an arrayed library of 405 *AGTR1* missense variants was successfully generated and validated by Oxford Nanopore long-read sequencing.

Sequencing confirmed both the integrity of the plasmid backbone and the correct nucleotide substitutions for every variant. Overall, the library achieved near-complete representation of known *AGTR1* mutational diversity, with 96.42% of intended missense variants successfully constructed.

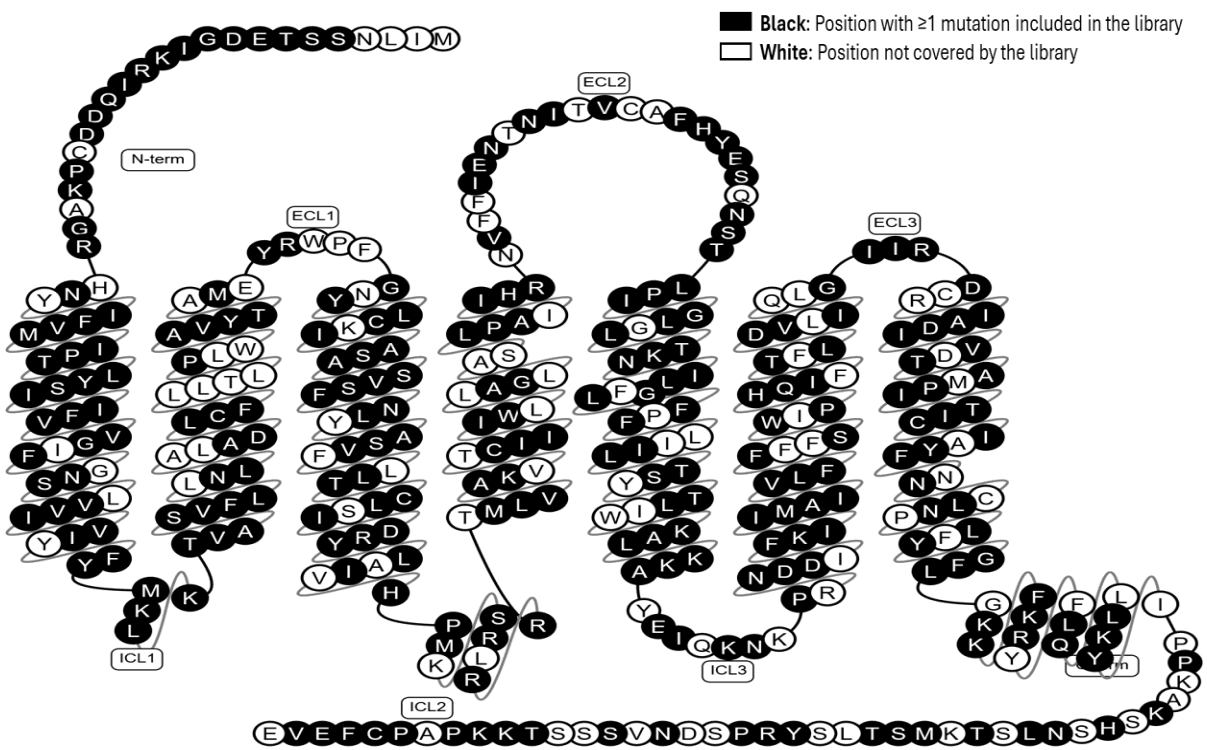

Figure 3 | **Snake plot representation of the *AGTR1* receptor illustrating the coverage of the generated missense variant library across all 359 amino acid positions.**

Each black circle indicates a variant that was successfully generated and arrayed, demonstrating near-complete representation of the missense variant landscape reported in gnomAD. White circles mark positions without variant coverage, corresponding to codons not reported to harbour missense variants in gnomAD, except at positions 2, 4 and 111. These uncovered positions resulted from an incorrect primer design, while position 207 uncovered position resulted from sampling limitations by screening only three out of the 25 colonies produced. Overall, the mutagenesis workflow achieved a 99.75% success rate.

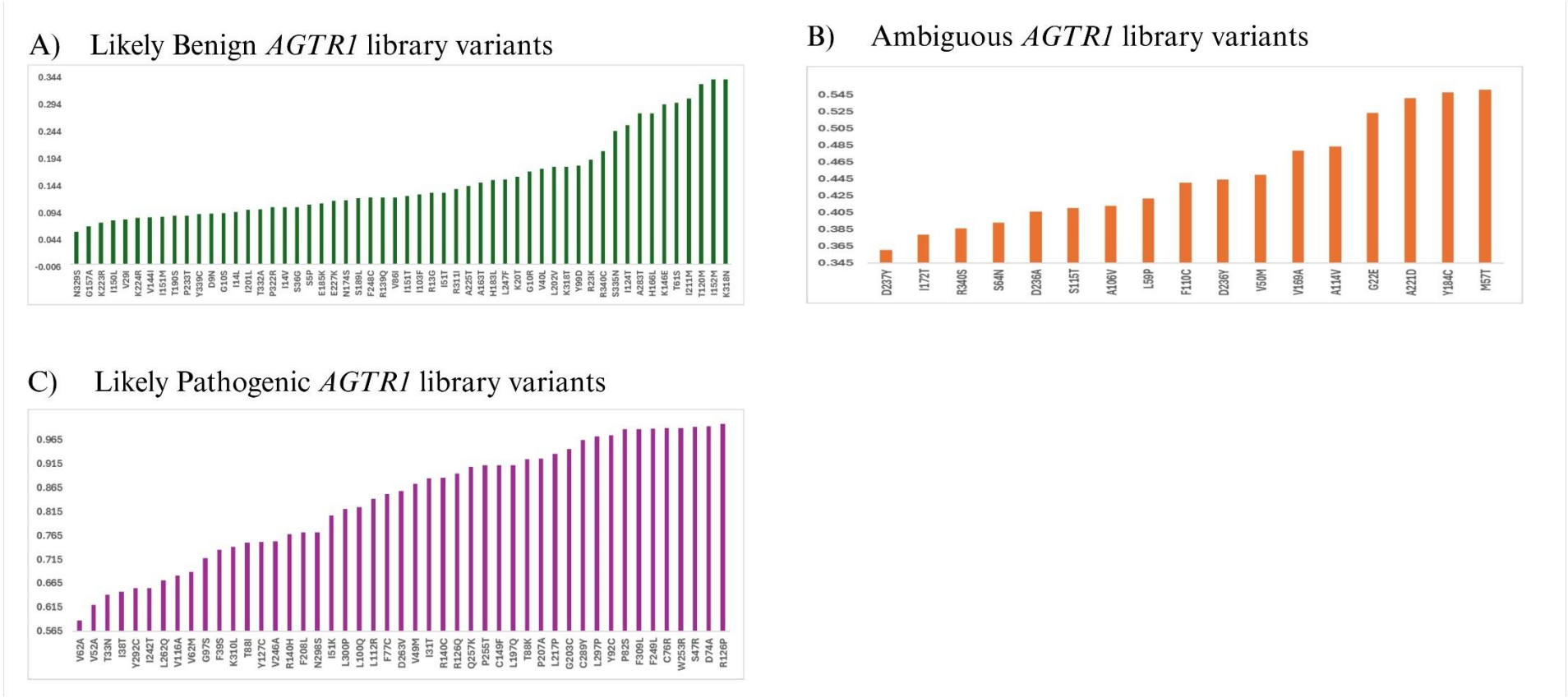

Figure 4 | **Grouping of *AGTR1* missense variant library by AlphaMissense pathogenicity prediction.**

Visual distribution of AlphaMissense pathogenicity scores for *AGTR1* missense variants cloned in the mutagenesis library, grouped by prediction functional category: (A) likely benign (scores ≤0.344), (B) ambiguous (scores 0.345-0.564) and (C) likely pathogenic (scores≥0.565). With the x-axis indicating the mutant substitution and the y-axis the corresponding AlphaMissense score.

III.3 SDM-PCR Mutagenesis Primers Validation and Construct Generation

Primer pairs for SDM PCR were designed in a way that each mutagenic primer (forward or reverse) was paired with its complementary counterpart targeting the opposite DNA strand. To evaluate the performance and reliability of the SDM-PCR workflow, a validation set of 13 variants distributed across the *AGTR1* open reading frame (I51M, S65G, F77I, S109R, R126Q, F182L, S189L, F206L, H256N, I276M, T332K, K351N and V358A) was randomly selected from all locations of the protein coding region and analysed by Sanger sequencing. Initial validation of the PCR amplification was carried out by agarose gel electrophoresis, which confirmed successful amplification of both complementary amplicons for selected variants (Figure 5A).

Sequencing analysis revealed that 11 of the 13 constructs contained the intended nucleotide substitution, while two variants (K351N and V358A) showed the WT sequence at the target site. These findings demonstrate the high fidelity and efficiency of the SDM PCR mutagenesis workflow in generating the *AGTR1* missense variants. Alignment of Sanger sequencing (Figure 5B) and chromatogram (Figure 5C) for representative WT and mutant clones further confirmed the accuracy and integrity of the introduced mutations.

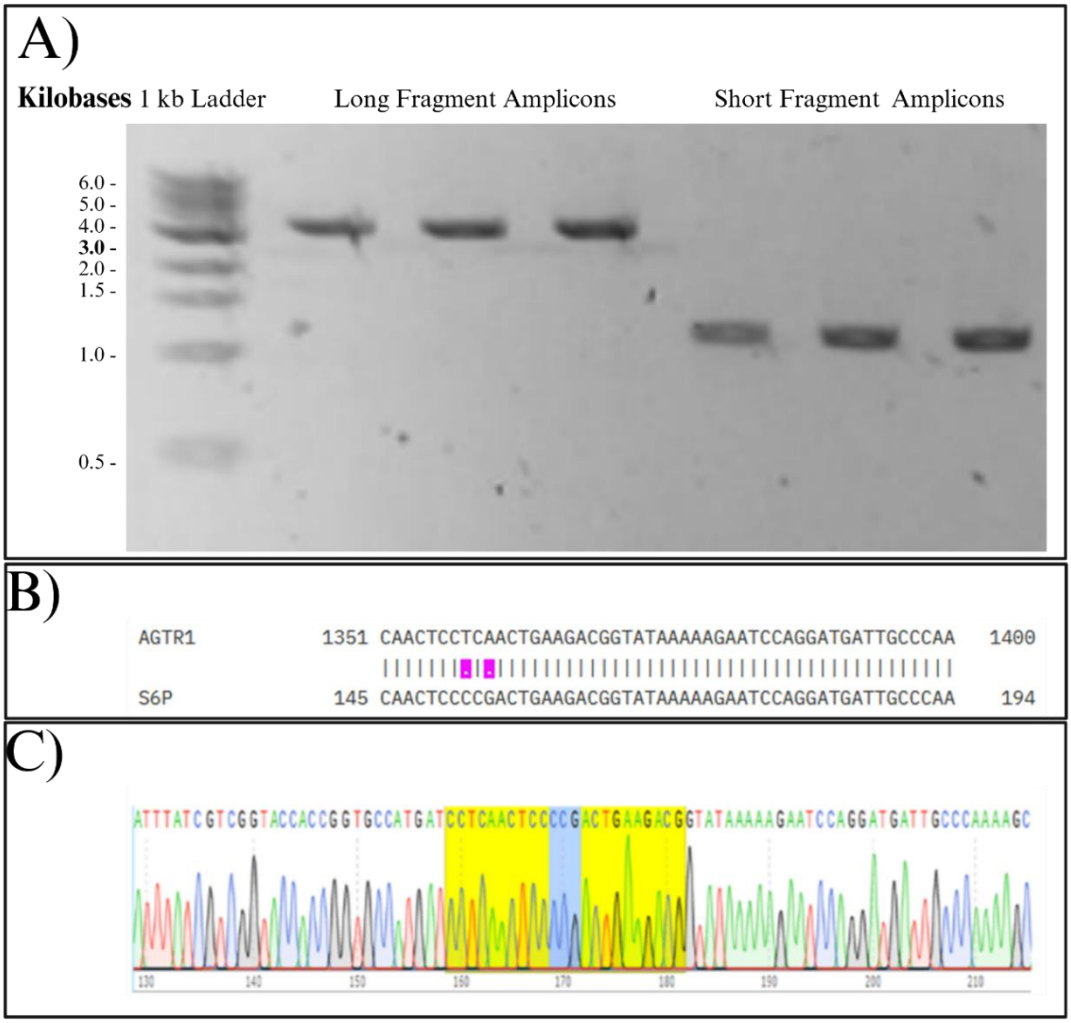

Figure 5 | **Representative successful site-directed mutagenesis PCR and two-fragment *in vivo* assembly.**

(A) Agarose gel electrophoresis showing expected SDM PCR products, confirming amplification. (B) Sequence alignment of the *AGTR1*_WT reference gene and the S6P mutant, the pink square indicates two nucleotide changes, representing the codon change from serine to proline. (C) Chromatogram from the Sanger sequencing result of S6P. Yellow highlights the region that corresponds to the primer sequence used for induced mutagenesis, and the blue region shows the nucleotide. Created in https://BioRender.com

III.4 Efficiency of SMD-PCR in *AGTR1* plasmid constructs

To evaluate the mutagenesis efficiency of the SDM PCR approach, both quantitative and qualitative metrics were assessed. Following transformation, CFUs were counted for each variant, and efficiency was calculated as the proportion of colonies carrying the desired nucleotide substitution. Colony formation was observed for nearly all the variants, with per-variant CFUs counts ranging from 2 to 183 colonies (Figure 6). However, a high colony count did not always correlate with mutagenesis success; some variants yielded numerous colonies but a low mutation rate, while others exhibited low colony counts yet a high proportion of correctly mutated clones.

Overall, mutagenesis success was robust, with 99.7% of variants containing at least one mutant clone. The only exception was variant P207A, which produced 25 colonies but showed no evidence of the desired mutation after next-generation sequencing, suggesting the possibility of off-target changes. Median CFU counts across variant groups produced around 50-60 colonies, although individual values varied widely, emphasising the consistency and robustness of the SDM PCR method employed.

Further analysis examined the relationship between primer GC content and mutagenesis success. Variants were compared against primer GC content and their mutation success rate from three colonies screened. Successful mutagenesis occurred across a broad GC content range 25% to nearly 80%. A high success rate (100%) was achieved in 251 variants regardless of primer GC content, intermediate (67%) success was observed in 128 variants, low (33%) success in 26 variants, and a single variant with (0%) success which had a primer GC content of 40%. These findings demonstrate that high-efficiency mutagenesis is attainable across diverse primer GC compositions.

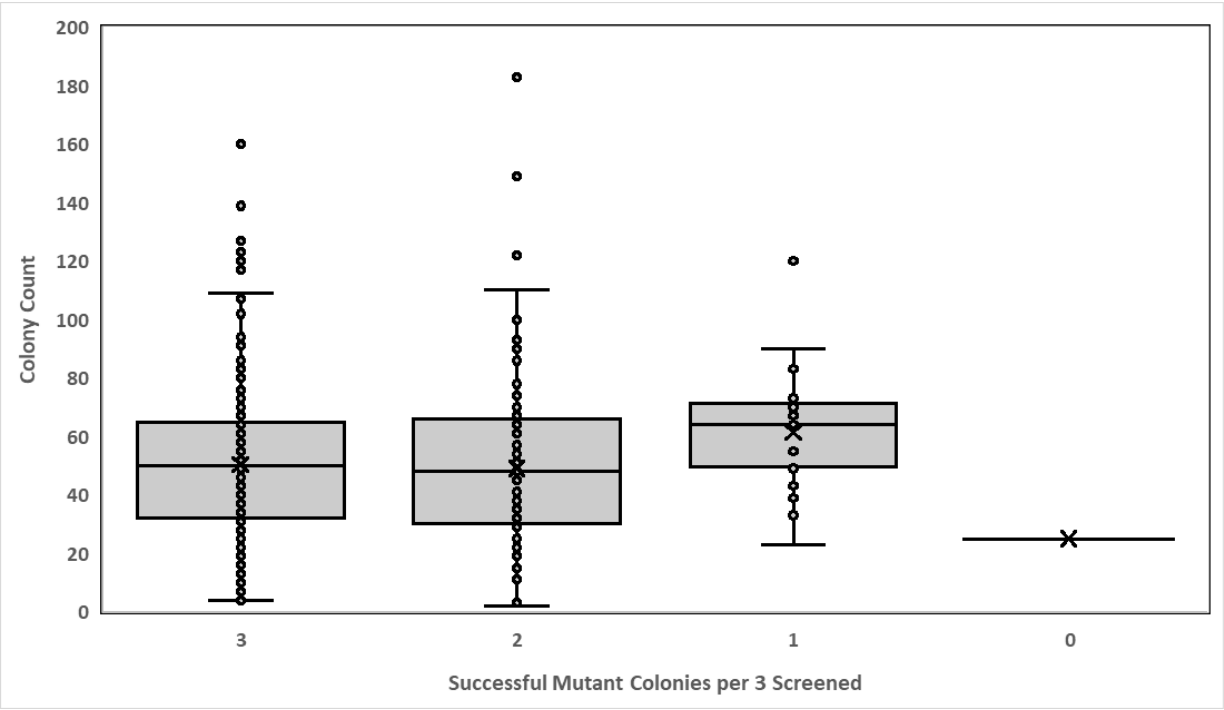

Figure 6 | **Correlation between total colonies and colonies containing the intended mutation.**

Box plot comparing colony count distribution across *AGTR1* SDM PCR variants grouped by the number of successful mutant colonies obtained per three screened colonies. Each box plot shows the colony count of variants yielding three, two, one or zero verified mutant colonies out of three picks. Boxes indicate the interquartile range, horizontal lines indicate de median, whiskers span the 10^{th} – 90^{th} percentiles, circles denote individual data points. The x marks the mean value for each category (n=406).

III.5 Optimisation and Validation of Calcium Assay

To enable robust and reproducible quantification of *AGTR1*-mediated calcium signalling. the assay was optimised to maximise signal quality and distinguish receptor-driven responses from background noise. Liquid injection can cause calcium assay artefacts due to activation of stretch receptors (Schleifenbaum *et al.*, 2014); therefore, we systematically tested a matrix of injection volumes (1-15 µL) at the lowest injection speed of 50 µL/s and well starting volumes from as low as 99µL up to 285 µL to assess their influence on *AGTR1* responses. These experiments demonstrated that *AGTR1*-expressing cells exhibited a stretch-induced activation upon injection of HBSS without Ca^{2+}, as observed in Figure 7. This shows the sensitivity of the assay to mechanical stimulation and highlights the need for optimisation of liquid parameters to prevent artefactual calcium signals.

A) Stretch-Induced Calcium Response in *AGTR1*-Expressing HEK293 Cells Following 5 µL HBSS (Ca^{2+}-Free) Injection into 195 µL Well Volume)

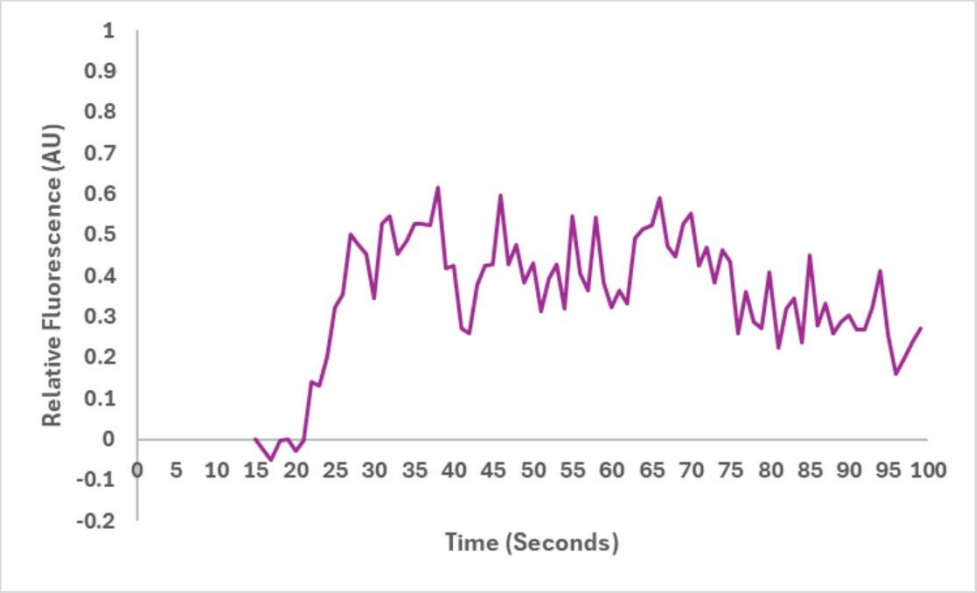

B) Stretch-Induced Calcium Response in *AGTR1*-Expressing HEK293 Cells Following 10 µL HBSS (Ca^{2+}-Free) Injection into 190 µL Well Volume)

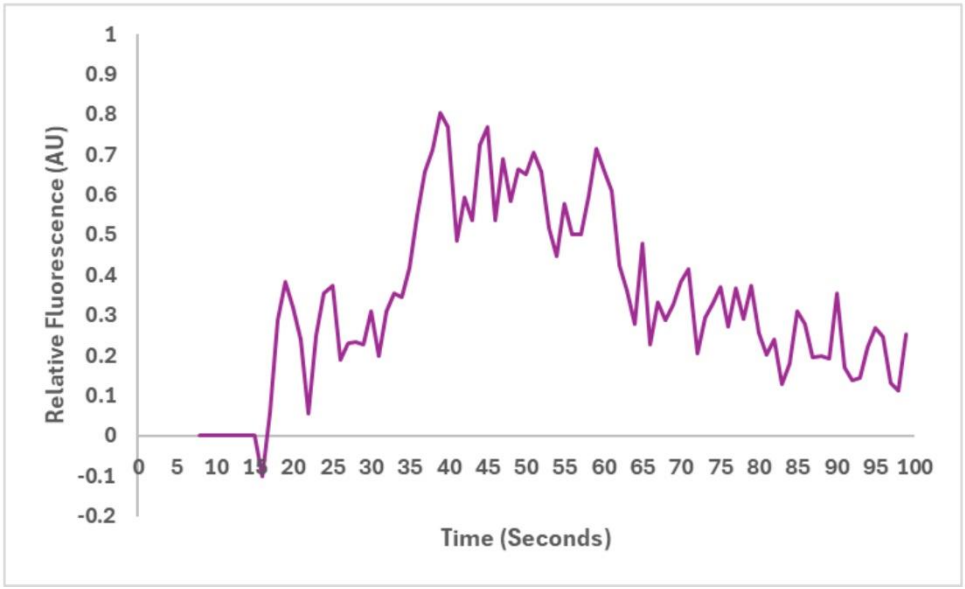

Figure 7 | **Stretch-induced calcium responses in *AGTR1*-expressing HEK293 cells.**

(A) mean normalised relative fluorescence traces from *AGTR1*-tranfescted HEK293 cells (n=3), following HBSS without Ca2+ injection of 5 µL into a 195 µL well volume. (B) mean normalised relative fluorescence traces from *AGTR1*-tranfescted HEK293 cells (n=3), following HBSS without Ca2+ injection of 10 µL into a 190 µL well volume. Both conditions showed an increase in relative fluorescence after injection at 13 seconds, independent of agonist addition. Created in https://BioRender.com

Experiments evaluated HEK293 cells transfected with *AGTR1* and non-transfected controls, challenged with varying concentrations of Ang II. Results confirmed dose-dependent fluorescence changes measured via Fluo-4 AM staining; however, negative controls showed elevated background signal, indicating injection artefacts (Figure 8).

A) Non-transfected HEK293 cells showing unexpected calcium response after 0.6 µM injection

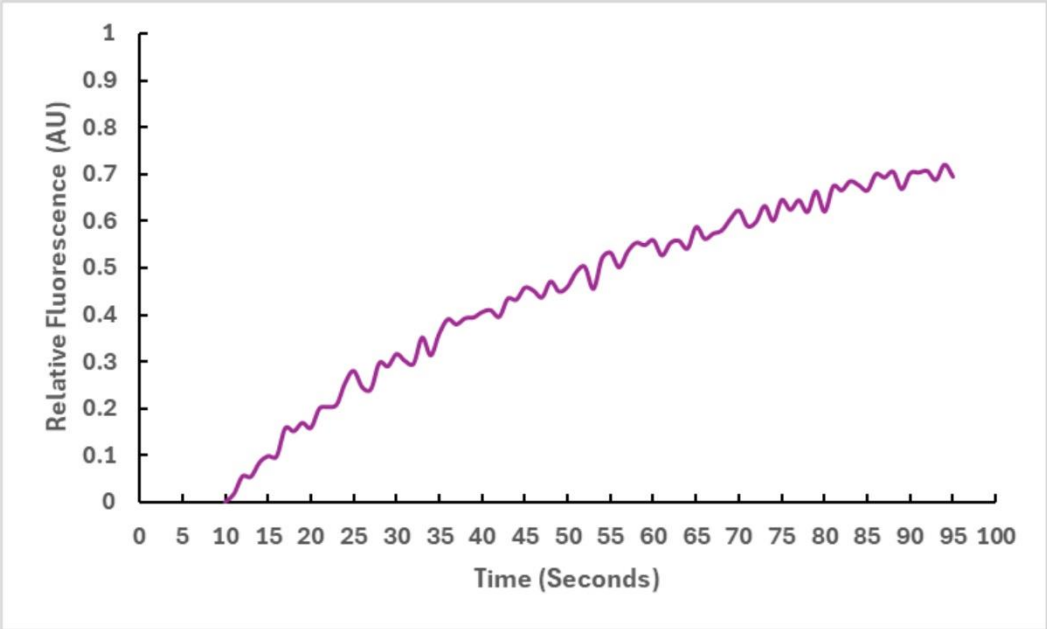

B) *AGTR1*-expressing HEK293 cells showing calcium response after 0.6 µM injection

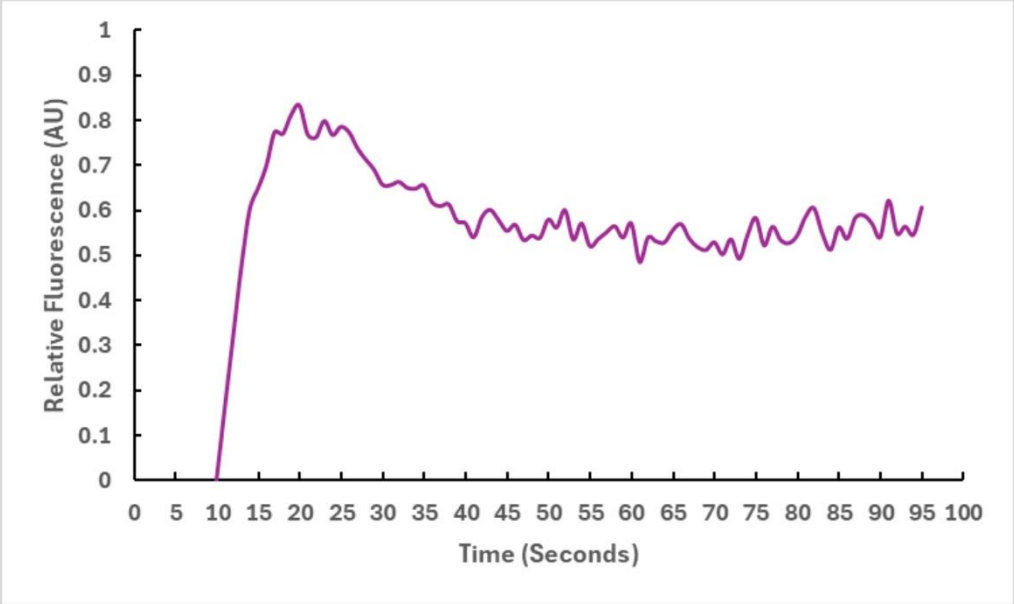

Figure 8 | **Calcium response to Ang II in non-transfected and *AGTR1*-expressing HEK293 cells.**

(A) Negative control relative fluorescence trace for non-transfected HEK293 cells following 0.6 µM AngII injection, showing an unexpected rise in intracellular calcium signal. (B) Relative fluorescence for *AGTR*-transfected HEK293 cells after 0.6 µM AngII injection, demonstrating receptor-mediated calcium signalling.

Screening combinations of injection volumes (1 µL) and well volumes (up to 199 µL) with the lowest injection speed (50 µL/s) revealed that the minimum injection volume into maximum well volume minimised background signals and variability between replicates (Figure 9). This configuration enabled clear discrimination of calcium signals from transfected versus non-transfected cells, reducing baseline noise and nonspecific response observed in dye-only controls.

A) Maximum calcium response (ΔMAX) in *AGTR1*-transfected and untransfected HEK293 cells at 199 µL well volume

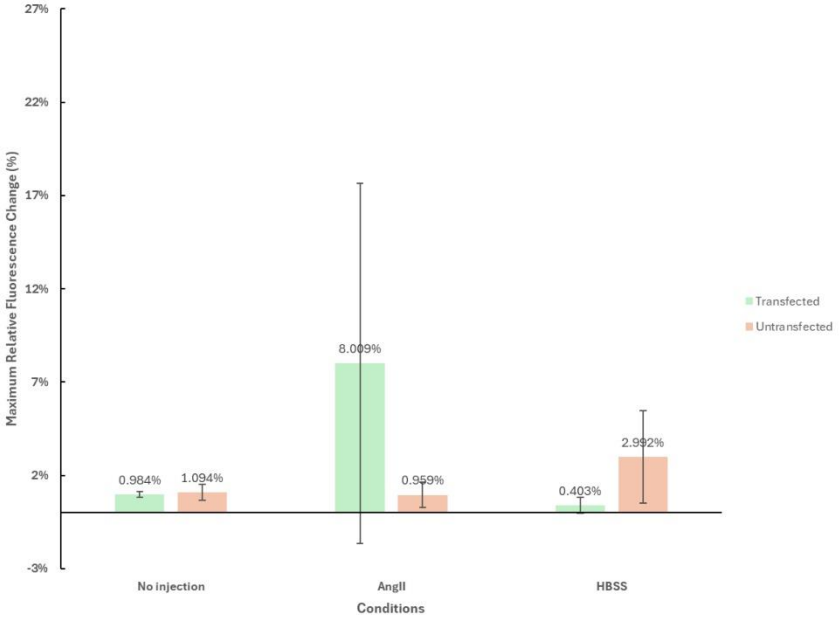

B) Maximum calcium response (ΔMAX) in *AGTR1*-transfected and untransfected HEK293 cells at 99 µL well volume

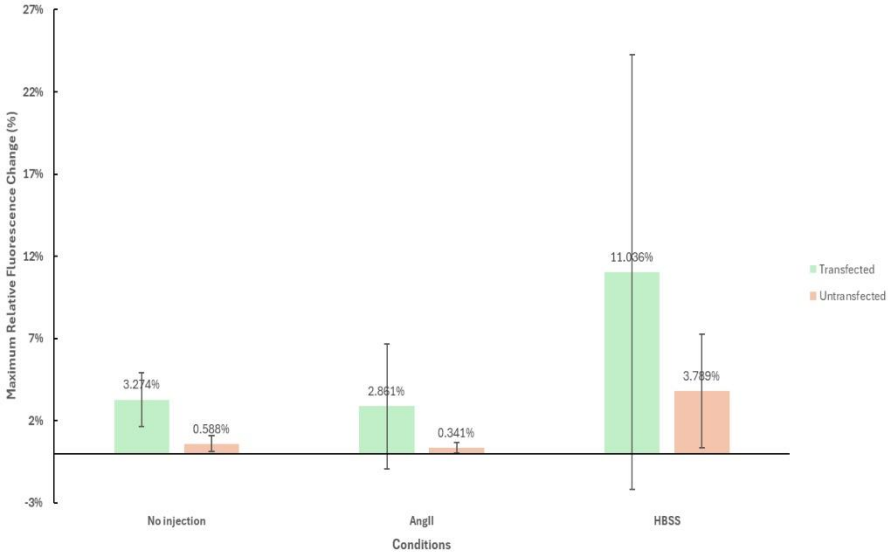

Figure 9 | **Maximum calcium response (ΔMAX) in *AGTR*1-transfected and non-transfected HEK293 cells under different well volume conditions.**

(A) Maximum relative fluorescence change in transfected and untransfected HEK293 cells for no injections, 1µL HBSS injections and 1 µL AngII stimulation (1 µM) at 199 µL well volume (with mean ± SD, n=3). (B) Bar graph showing the same conditions for 99 µL well volume. Results demonstrate that the optimal condition assay is 199 µL well volume and 1 µL injection.

Validation assays using optimised settings (199 µL well volume, 1 µL agonist injection) produced a clear fluorescence peak in *AGTR1*-transfected cells with minimal background in controls. The representative traces are shown in Figure 10. Illustrate a kinetic calcium response with a well-defined rise and decay. Coefficient of variation and maximum signal change analyses confirmed reproducibility and sensitivity. The time to peak fluorescence (Tmax) was after for *AGTR1*-transfected cells compared to controls.

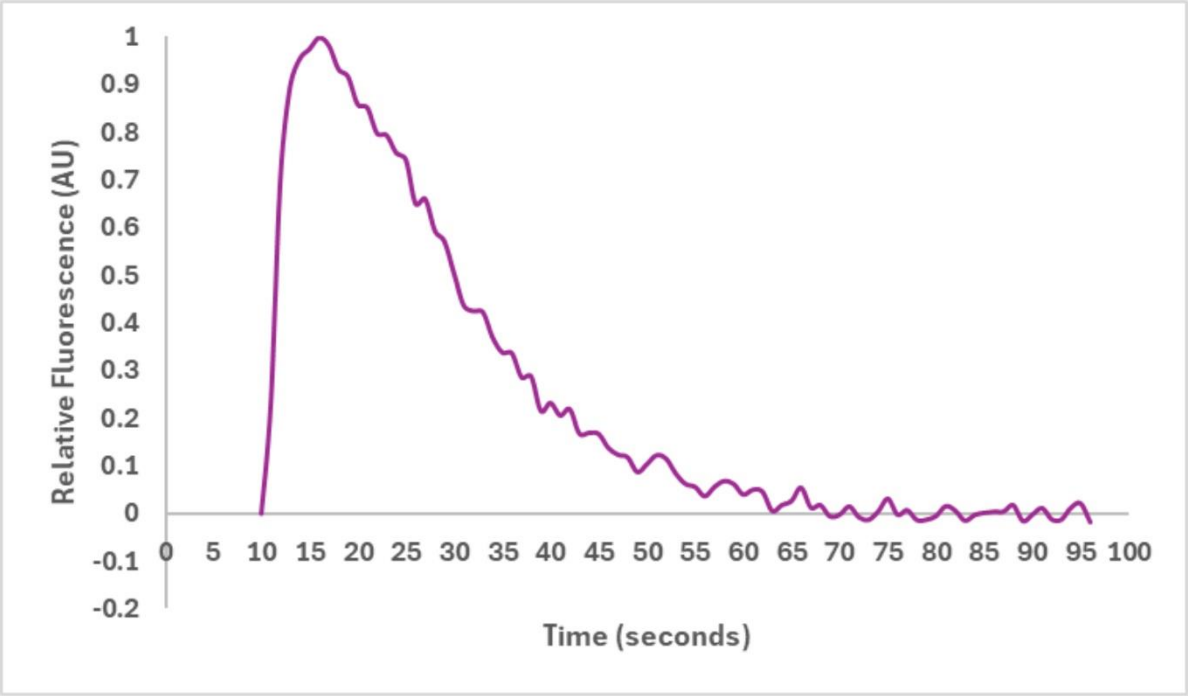

Figure 10 | **Representative kinetic calcium response trace in *AGTR1*-transfected HEK293 cell.**

Kinetic calcium response under optimised conditions of 1 µL AngII (1 µM) and 199 µL well volume.

Chapter IV: Discussion

This thesis addresses an important question in pharmacogenomics: how genetic variation in the *AGTR1* gene contributes to functional diversity in Ang II signalling, potentially influencing individual drug responses, how extensively known *AGTR1* missense variants can be captured in a high-throughput generated library, and to establish whether such resources can support large-scale high-throughput functional pharmacogenomic studies. This project successfully generated the largest *AGTR1* missense variant library to date, encompassing 405 arrayed variants derived from gnomAD and the literature, representing a cumulative allele frequency of 0.83%, corresponding to an estimated 135 million carriers worldwide. This library fully covers the wide spectrum of *AGTR1* variants, including the neglected 1.65% for which the medications are not tailored, with an efficient high-throughput SDM-PCR and cloning workflow, demonstrating that functional interrogation of GPCRs coding variation is technically feasible and scalable.

The wide coverage of documented coding diversity in *AGTR1* has been captured for systematic functional testing, rather than the small and biased variants selected in other studies. This change AGTR1 pharmacogenomics from a one-size-fits-all approach toward a more comprehensive, case-by-case, atlas-like source of receptor variation, enabling genotype-phenotype relationships to be explored across the full spectrum of population frequencies, going from low to common frequencies of alleles. At the same time, as we know more about these receptors and the addition of an increasingly rare population of variants expanding existing databases, these library studies need to be dynamic rather than a definitive endpoint.

A central innovation was the development of a scalable and adaptable SDM PCR workflow combined with a two-fragment assembly method that leverages *E. coli*, endogenous homologous recombination machinery, which achieved an overall mutagenesis success rate of 99.7%. By using low parental template input, high-throughput colony screening in 96-well format, and long-read sequencing for full-length verification, the pipeline substantially reduces labour and cost compared with traditional QuickChange-style mutagenesis. In comparison with recent approaches such as the P3 method by Mousavi *et al.* (2025), our workflow uses slightly bigger reaction volumes but markedly lower parental DNA, more compact culture formats and shorter incubation times, together supporting higher throughput and resource efficiency. Making it realistic to extend this strategy to other GPCRs and clinically relevant receptors.

Regular AGTR1 functional studies have focused on a small number of variants, often selected for prior clinical association or specific interest, limiting the ability to generate findings for the broader variant landscape. By contrast, the present library is built directly from population genetic datasets for an unbiased functional screening, allowing deeper studies to identify patterns such as tolerance of particular regions to substitution or enrichment of deleterious variants in specific domains to be mapped systematically once further assays are conducted.

Key strengths of this project include the complete coverage of currently known AGTR1 missense variants, the high mutagenesis success rate, and the use of long-read sequencing for comprehensive plasmid validation, which together minimise the risk of undetected background mutations. The modular nature of primer design, barcoding, and pooling strategies also means that the workflow can be readily adapted or expanded as new variants are identified. Future work should focus on coupling this library to multiplexed functional screening to generate quantitative maps of how individual variants affect Ang II signalling and receptor expression. Integration of these functional profiles with clinical and genetic datasets would allow testing of whether specific functional classes of variants correlate with blood pressure response and/or adverse drug reactions.

IV. 3 Conclusion

This thesis produced the most extensive and comprehensive *AGTR1* missense variant library to date, to my current knowledge. Constructed using an innovative, high-throughput molecular engineering pipeline. By covering all reported missense variants in gnomAD, this project library provides a valuable tool for testing and understanding functional diversity in *AGTR1* and it pharmacogenomic implications. The pipeline used in this project is oriented for scalability and efficiency, paving the ground for future studies to investigate the genotype-phenotype relationships and facilitating high-throughput functional analysis of genetic variations for this important GPCR and other GPCRs. While future work is required, this project provides a robust platform that integrates molecular techniques and population genomics toward advancing receptor biology research.

References

Agostini, L. d. C., Silva, N. N. T., Belo, V. d. A., Luizon, M. R., Lima, A. A., & da Silva, G. N. (2024). Pharmacogenetics of angiotensin-converting enzyme inhibitors (ACEI) and angiotensin II receptor blockers (ARB) in cardiovascular diseases. *European Journal of Pharmacology*, *981*, 176907. https://doi.org/https://doi.org/10.1016/j.ejphar.2024.176907

Al-Makki, A., DiPette, D., Whelton, P. K., Murad, M. H., Mustafa, R. A., Acharya, S., Beheiry, H. M., Champagne, B., Connell, K., Cooney, M. T., Ezeigwe, N., Gaziano, T. A., Gidio, A., Lopez-Jaramillo, P., Khan, U. I., Kumarapeli, V., Moran, A. E., Silwimba, M. M., Rayner, B.,…Khan, T. (2022). Hypertension Pharmacological Treatment in Adults: A World Health Organization Guideline Executive Summary. *Hypertension (Dallas, Tex. 1979)*, *79*(1), 293-301. https://doi.org/10.1161/HYPERTENSIONAHA.121.18192

Alberts, B., Johnson, A., Julian Lewis, M. R., Roberts, K., & Walter, P. (2002). *Molecular Biology of the Cell. 4th edition.* https://www.ncbi.nlm.nih.gov/books/NBK26818/

Atkins, E. R., Nguyen, L. H., Chatterton, M. L., Schlaich, M., Schutte, A. E., & Rodgers, A. (2024). The cost of treating hypertension in Australia, 2012–22: an economic analysis. *Medical Journal of Australia*, *221*(11), 612-616.

Auger-Messier, M., Clement, M., Lanctot, P. M., Leclerc, P. C., Leduc, R., Escher, E., & Guillemette, G. (2003). The constitutively active N111G-AT1 receptor for angiotensin II maintains a high affinity conformation despite being uncoupled from its cognate G protein Gq/11α. *Endocrinology*, *144*(12), 5277-5284.

Billet, S., Bardin, S., Verp, S., Baudrie, V., Michaud, A., Conchon, S., Muffat-Joly, M., Escoubet, B., Souil, E., & Hamard, G. (2007). Gain-of-function mutant of angiotensin II receptor, type 1A, causes hypertension and cardiovascular fibrosis in mice. *The Journal of clinical investigation*, *117*(7), 1914-1925.

Carrigan, P. E., Ballar, P., & Tuzmen, S. (2011). Site-directed mutagenesis. *Methods Mol Biol*, *700*, 107-124. https://doi.org/10.1007/978-1-61737-954-3_8

Dzau, V. J., & Hodgkinson, C. P. (2024). Precision Hypertension. *Hypertension*, *81*(4), 702-708. https://doi.org/10.1161/hypertensionaha.123.21710

Gilman, A. G. (1987). G Proteins: Transducers of Receptor-Generated Signals. *Annual review of biochemistry*, *56*(1), 615-649. https://doi.org/10.1146/annurev.bi.56.070187.003151

Glazer, A. M., Tabet, D. R., Parikh, V. N., Kroncke, B. M., Cote, A. G., Yamamoto, Y., Wang, Q., Muhammad, A., Lancaster, M. C., O'Neill, M. J., Weile, J., Yang, T., Macrae, C. A., Ashley, E. A., Roth, F. P., & Roden, D. M. (2025). Creating an atlas of variant effects to resolve variants of uncertain significance and guide cardiovascular medicine. *Nat Rev Cardiol*. https://doi.org/10.1038/s41569-025-01201-7

Gocal, G. F., Schöpke, C., & Beetham, P. R. (2015). Oligo-mediated targeted gene editing. In *Advances in new technology for targeted modification of plant genomes* (pp. 73-89). Springer.

Goodfriend, T. L., Elliott, M. E., & Catt, K. J. (1996). Angiotensin Receptors and Their Antagonists. *The New England journal of medicine*, *334*(25), 1649-1655. https://doi.org/10.1056/NEJM199606203342507

Grimson, S., Cox, A. J., Pringle, K. G., Burns, C., Lumbers, E. R., Blackwell, C. C., & Scott, R. J. (2016). The prevalence of unique SNP s in the renin-angiotensin system highlights the need for pharmacogenetics in Indigenous Australians. *Clinical and Experimental Pharmacology and Physiology*, *43*(2), 157-160.

Hansen, J. L., Haunsø, S., Brann, M. R., Sheikh, S. P., & Weiner, D. M. (2004). Loss-of-Function Polymorphic Variants of the Human Angiotensin II Type 1 Receptor. *Molecular Pharmacology*, *65*(3), 770-777. https://doi.org/https://doi.org/10.1124/mol.65.3.770

Heng, J., Hu, Y., Pérez-Hernández, G., Inoue, A., Zhao, J., Ma, X., Sun, X., Kawakami, K., Ikuta, T., Ding, J., Yang, Y., Zhang, L., Peng, S., Niu, X., Li, H., Guixà-González, R., Jin, C., Hildebrand, P. W., Chen, C., & Kobilka, B. K. (2023). Function and dynamics of the intrinsically disordered carboxyl terminus of β2 adrenergic receptor. *Nat Commun*, *14*(1), 2005. https://doi.org/10.1038/s41467-023-37233-1

Herger, M., Kajba, C. M., Buckley, M., Cunha, A., Strom, M., & Findlay, G. M. (2025). High-throughput screening of human genetic variants by pooled prime editing. *Cell Genomics*, *5*(4).

Hou, T., Yu, L., Shi, X., Zhen, Y., Ji, L., Wei, Z., & Xu, Y. (2024). Pharmacogenomics assists in controlling blood pressure in cardiovascular and cerebrovascular patients during

Rehabilitation: a case report [Case Report]. *Frontiers in Pharmacology*, *Volume 15 - 2024*. https://doi.org/10.3389/fphar.2024.1424683

Huang, F., Spangler, J. R., & Huang, A. Y. (2017). In vivo cloning of up to 16 kb plasmids in E. coli is as simple as PCR. *PloS one*, *12*(8), e0183974.

Hubbard, K. B., & Hepler, J. R. (2006). Cell signalling diversity of the Gqα family of heterotrimeric G proteins. *Cellular signalling*, *18*(2), 135-150.

Iqbal, Z., & Sadaf, S. (2022). Forty years of directed evolution and its continuously evolving technology toolbox: A review of the patent landscape. *Biotechnology and Bioengineering*, *119*(3), 693-724.

Israr, H., Sibghat, A., Baig, F., Gul, W., Jalil, F., & Khan, N. (2025). Functional Characterization of Non-Synonymous SNPs in the Hypertension-Associated AGT Gene Using Bioinformatic Tools. *Journal of Health, Wellness and Community Research*, e776-e776.

Katherine Chao, g. P. T. (2023). *gnomAD v4.0* (Version 4.0). https://gnomad.broadinstitute.org/news/2023-11-gnomad-v4-0/

Kawai, T., Forrester, S. J., O'Brien, S., Baggett, A., Rizzo, V., & Eguchi, S. (2017). AT1 receptor signaling pathways in the cardiovascular system. *Pharmacol Res*, *125*(Pt A), 4-13. https://doi.org/10.1016/j.phrs.2017.05.008

Khehra, N., Padda, I. S., & Zubair, M. (2025). Polymerase Chain Reaction (PCR). In *StatPearls*. StatPearls Publishing

Krenn, M., Schmidt, A., Wagner, M., Ernst, M., Graf, E., Zulehner, G., Cetin, H., Zimprich, F., & Rath, J. (2025). AlphaMissense prediction for the evaluation of missense variants in the diagnostic setting of neuromuscular disorders. *Journal of Neuromuscular Diseases*, *0*(0), 22143602251370957. https://doi.org/10.1177/22143602251370957

Lefkowitz, R. J., & Shenoy, S. K. (2005). Transduction of receptor signals by β-arrestins. *Science*, *308*(5721), 512-517.

Liu, S., Anderson, P. J., Rajagopal, S., Lefkowitz, R. J., & Rockman, H. A. (2024). G Protein-Coupled Receptors: A Century of Research and Discovery. *Circ Res*, *135*(1), 174-197. https://doi.org/10.1161/circresaha.124.323067

Lu, W.-l., Yuan, J.-h., Liu, Z.-y., Su, Z.-H., Shen, Y.-C., Li, S.-j., & Zhang, H. (2023). Worldwide trends in mortality for hypertensive heart disease from 1990 to 2019 with projection to 2034: data from the Global Burden of Disease 2019 study. *European Journal of Preventive Cardiology*, *31*(1), 23-37. https://doi.org/10.1093/eurjpc/zwad262

Mahjour, B., Zhang, R., Shen, Y., McGrath, A., Zhao, R., Mohamed, O. G., Lin, Y., Zhang, Z., Douthwaite, J. L., Tripathi, A., & Cernak, T. (2023). Rapid planning and analysis of high-throughput experiment arrays for reaction discovery. *Nature Communications*, *14*(1), 3924. https://doi.org/10.1038/s41467-023-39531-0

Mahoney, J. P., & Sunahara, R. K. (2016). Mechanistic insights into GPCR–G protein interactions. *Current Opinion in Structural Biology*, *41*, 247-254. https://doi.org/https://doi.org/10.1016/j.sbi.2016.11.005

Mauzy, C. A., Hwang, O., Egloff, A. M., Wu, L. H., & Chung, F. Z. (1992). Cloning, expression, and characterization of a gene encoding the human angiotensin II type 1A receptor. *Biochem Biophys Res Commun*, *186*(1), 277-284. https://doi.org/10.1016/s0006-291x(05)80804-6

Moerschell, R. P., Tsunasawa, S., & Sherman, F. (1988). Transformation of yeast with synthetic oligonucleotides. *Proceedings of the National Academy of Sciences*, *85*(2), 524-528. https://doi.org/doi:10.1073/pnas.85.2.524

Mousavi, N., Zhou, E., Razavi, A., Ebrahimi, E., Varela-Castillo, P., & Yang, X. J. (2025). P3 site-directed mutagenesis: An efficient method based on primer pairs with 3'-overhangs. *J Biol Chem*, *301*(3), 108219. https://doi.org/10.1016/j.jbc.2025.108219

Oakley, R. H., Laporte, S. A., Holt, J. A., Caron, M. G., & Barak, L. S. (2000). Differential affinities of visual arrestin, βarrestin1, and βarrestin2 for G protein-coupled receptors delineate two major classes of receptors. *Journal of biological chemistry*, *275*(22), 17201-17210.

Oro, C., Qian, H., & Thomas, W. G. (2007). Type 1 angiotensin receptor pharmacology: Signaling beyond G proteins. *Pharmacology & therapeutics*, *113*(1), 210-226. https://doi.org/https://doi.org/10.1016/j.pharmthera.2006.10.001

Pierce, K. L., Premont, R. T., & Lefkowitz, R. J. (2002). Seven-transmembrane receptors. *Nature Reviews Molecular Cell Biology*, *3*(9), 639-650. https://doi.org/10.1038/nrm908

Poudel, B., Tatikonda, R. R., & Vanegas, J. M. (2023). Mechanical vs. agonist induced activation in the angiotensin II type 1 receptor. *Biophysical Journal*, *122*(3, Supplement 1), 92a. https://doi.org/https://doi.org/10.1016/j.bpj.2022.11.695

Schleifenbaum, J., Kassmann, M., Szijártó, I. A., Hercule, H. C., Tano, J.-Y., Weinert, S., Heidenreich, M., Pathan, A. R., Anistan, Y.-M., Alenina, N., Rusch, N. J., Bader, M., Jentsch, T. J., & Gollasch, M. (2014). Stretch–Activation of Angiotensin II Type 1_a Receptors Contributes to the Myogenic Response of Mouse Mesenteric and Renal Arteries. *Circulation Research*, *115*(2), 263-272. https://doi.org/doi:10.1161/CIRCRESAHA.115.302882

Schutte, A. E., Jafar, T. H., Poulter, N. R., Damasceno, A., Khan, N. A., Nilsson, P. M., Alsaid, J., Neupane, D., Kario, K., Beheiry, H., Brouwers, S., Burger, D., Charchar, F. J., Cho, M.-C., Guzik, T. J., Haji Al-Saedi, G. F., Ishaq, M., Itoh, H., Jones, E. S. W.,…Tomaszewski, M. (2022). Addressing global disparities in blood pressure control: perspectives of the International Society of Hypertension. *Cardiovascular Research*, *119*(2), 381-409. https://doi.org/10.1093/cvr/cvac130

Seravalle, G., & Grassi, G. (2023). Renin–angiotensin–aldosterone system and blood pressure regulation. In *Endocrine Hypertension* (pp. 63-75). Elsevier.

Shacham, S., Marantz, Y., Bar-Haim, S., Kalid, O., Warshaviak, D., Avisar, N., Inbal, B., Heifetz, A., Fichman, M., & Topf, M. (2004). PREDICT modeling and in-silico screening for G-protein coupled receptors. *Proteins: Structure, Function, and Bioinformatics*, *57*(1), 51-86.

Simon, M. I., Strathmann, M. P., & Gautam, N. (1991). Diversity of G proteins in signal transduction. *Science*, *252*(5007), 802-808.

Sprang, S. R., Chen, Z., & Du, X. (2007). Structural Basis of Effector Regulation and Signal Termination in Heterotrimeric Gα Proteins. In *Advances in Protein Chemistry* (Vol. 74, pp. 1-65). Academic Press. https://doi.org/https://doi.org/10.1016/S0065-3233(07)74001-9

Su, C., Xue, J., Ye, C., & Chen, A. (2021). Role of the central renin-angiotensin system in hypertension. *International journal of molecular medicine*, *47*(6), 95.

Tsunoda, S., Sierralta, J., Sun, Y., Bodner, R., Suzuki, E., Becker, A., Socolich, M., & Zuker, C. S. (1997). A multivalent PDZ-domain protein assembles signalling complexes in a G-protein-coupled cascade. *Nature*, *388*(6639), 243-249. https://doi.org/10.1038/40805

Valentine, W. J., & Tigyi, G. (2012). High-throughput assays to measure intracellular Ca^{2+} mobilization in cells that express recombinant S1P receptor subtypes. *Methods Mol Biol*, *874*, 77-87. https://doi.org/10.1007/978-1-61779-800-9_7

Verma, N., Rastogi, S., Chia, Y. C., Siddique, S., Turana, Y., Cheng, H. M., Sogunuru, G. P., Tay, J. C., Teo, B. W., Wang, T. D., Tsoi, K. K. F., & Kario, K. (2021). Non-pharmacological management of hypertension. *J Clin Hypertens (Greenwich)*, *23*(7), 1275-1283. https://doi.org/10.1111/jch.14236

World Health Organization. (2025). *Uncontrolled high blood pressure puts over a billion people at risk*. https://www.who.int/news/item/23-09-2025-uncontrolled-high-blood-pressure-puts-over-a-billion-people-at-risk

Yasi, E. A., Kruyer, N. S., & Peralta-Yahya, P. (2020). Advances in G protein-coupled receptor high-throughput screening. *Curr Opin Biotechnol*, *64*, 210-217. https://doi.org/10.1016/j.copbio.2020.06.004

Yin, J.-A., Frick, L., Scheidmann, M. C., Liu, T., Trevisan, C., Dhingra, A., Spinelli, A., Wu, Y., Yao, L., Vena, D. L., Knapp, B., Guo, J., De Cecco, E., Ging, K., Armani, A., Oakeley, E. J., Nigsch, F., Jenzer, J., Haegele, J.,…Aguzzi, A. (2025). Arrayed CRISPR libraries for the genome-wide activation, deletion and silencing of human protein-coding genes. *Nature Biomedical Engineering*, *9*(1), 127-148. https://doi.org/10.1038/s41551-024-01278-4

Zaman, M. A., Oparil, S., & Calhoun, D. A. (2002). Drugs targeting the renin–angiotensin–aldosterone system. *Nature reviews Drug discovery*, *1*(8), 621-636.

Zeghal, M., Laroche, G., Freitas, J. D., Wang, R., & Giguère, P. M. (2023). Profiling of basal and ligand-dependent GPCR activities by means of a polyvalent cell-based high-throughput platform. *Nature Communications*, *14*(1), 3684. https://doi.org/10.1038/s41467-023-39132-x

Zhang, D., Liu, Y., Zaidi, S. A., Xu, L., Zhan, Y., Chen, A., Guo, J., Huang, X. P., Roth, B. L., & Katritch, V. (2023). Structural insights into angiotensin receptor signaling modulation by balanced and biased agonists. *The EMBO journal*, *42*(11), e112940.

Zheng, X., Xing, X.-H., & Zhang, C. (2017). Targeted mutagenesis: A sniper-like diversity generator in microbial engineering. *Synthetic and Systems Biotechnology*, *2*(2), 75-86. https://doi.org/https://doi.org/10.1016/j.synbio.2017.07.001

Zhu, P., Lu, H., Jing, Y., Zhou, H., Ding, Y., Wang, J., Guo, D., Guo, Z., & Dong, C. (2019). Interaction Between AGTR1 and PPARγ Gene Polymorphisms on the Risk of Nonalcoholic Fatty Liver Disease. *Genetic Testing and Molecular Biomarkers*, *23*(3), 166-175. https://doi.org/10.1089/gtmb.2018.0203

Ziaja, M., Urbanek, K. A., Kowalska, K., & Piastowska-Ciesielska, A. W. (2021). Angiotensin II and Angiotensin Receptors 1 and 2—Multifunctional System in Cells Biology, What Do We Know? *Cells*, *10*(2), 381. https://www.mdpi.com/2073-4409/10/2/381

Perplexity AI. (2025). *Perplexity.ai* [Large language model]. https://www.perplexity.ai/

AI Use Acknowledgment

Perplexity AI was utilised as a brainstorming tool to generate ideas and provide structure suggestions for document organisation and enhancing clarity. Grammarly AI was employed to improve sentence structure and grammatical accuracy for polished writing. The original draft content was authored by Felipe de Jesus Navarro Vela, with knowledge from other authors incorporated with proper acknowledgement to the original source.

V. Appendix

Table 1 | **Thermocycler steps and conditions for excising the mCherry fluorescent fusion protein from the *AGTR1* plasmid.**

Thermal cycling parameters used during excising the mCherry fluorescent fusion protein from the *AGTR1* plasmid.

Step	Temperature (°C)	Time	Cycles
Initial denaturation	98	30 seconds	1
Denaturation	98	55 seconds	28
Aneealing	55	2 minutes	28
Extension	72	2 minutes	28
Final extension	72	7 minutes	1
Hold	12	Indefinite	-

Table 2 | **Primer sequences used for excising the mCherry fluorescent fusion protein.**

List of the primer names and their corresponding sequence used during mCherry removal.

Primer Name	Sequence
OJ107	GCACCATGTTTCGAGGTCGAATAAGGATCCTGATCATCGAAATTTAAGC
OJ108	GCTTAAATTTCGATGATCAGGATCCTTATTCGACCTCGAAACATGGTGC
SDM1R	CTGTTTTTGCTCACCCAGAAACG
SDM1F	CGTTTCTGGGTGAGCAAAAACAG

Table 3 | **Thermocycler steps and conditions for Site-Directed Mutagenesis.**

Thermal cycling parameters used during SDM-PCR to amplify mutant *AGTR1* constructs.

Step	Temperature (°C)	Time	Cycles
Initial denaturation	95	3 minutes	1
Denaturation	95	30 seconds	28
Aneealing	55	30 seconds	28
Extension	72	2 minutes 12 seconds (1kb/min)	28
Final extension	72	15 minutes	1
Hold	4	Indefinite	-

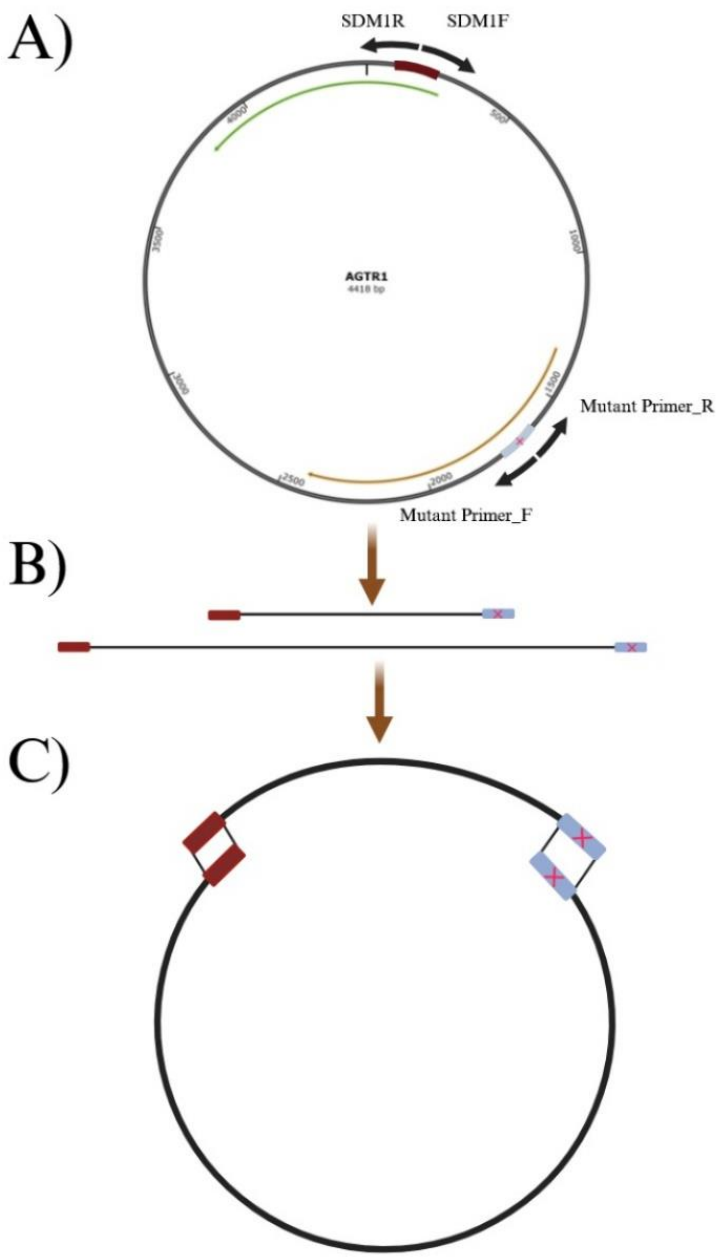

Figure 11 | **Visualisation of Site-Directed Mutagenesis (SDM) PCR workflow.**

(A) *AGTR1* template plasmid used for introduction of specific mutation, (Green arrow) indicates the ampicillin resistant sequence, (Gold arrow) indicates *AGTR1* encoding sequence, SDM1R/SDM1F are designed primers to anneal in the ampicillin region, Mutant Primer_F/R incorporate the nucleotide mismatch to induce the single amino acid substitution. The amplification occurs in two separate PCR reactions, each generating one of the two overlapping amplicons. SMD1F/Mutant primer_R amplifies in the 5' to 3' direction, while SDM1R/Mutant primer_F amplifies the complementary strand from 3' to 5'. (B) Linear PCR products containing overlapping sequence and the intended mutation (Red cross). (C) In vivo 2-Fragment assembly using endogenous homologous recombination machinery in E. coli. Created in https://BioRender.com

Table 4 | **Primer names and corresponding sequence for PCR barcoding.**

List of all primers used for PCR barcoding and their respective sequences. PBJ1, 2, and 3 are unique forward primers used in combination with PBJ_Fwd_uni. The bold region of the sequence for PBJ1, 2, and 3 are reverse complement of the 3' UTR of the plasmid sequence, and PBJ_Fwd_uni is the 5' UTR of the plasmid sequence.

Primer Name	Sequence
PBJ1 (PacBio 16S_Rev_42)	AAGCAGTGGTATCAACGCAGAGTCACGACGAC**GATGGCTGGCAACTAGAAG**
PBJ2 (PacBio 16S_Rev_43)	AAGCAGTGGTATCAACGCAGAGCGAGTCTAGC**GATGGCTGGCAACTAGAAG**
PBJ3 (PacBio 16S_Rev_44)	AAGCAGTGGTATCAACGCAGAGCAGCAGTGAC**GATGGCTGGCAACTAGAAG**
PBJ_Fwd_uni (PacBio 16S_Fwd_12)	CTACACGACGCTCTTCCGATCTGTAGACGCTG**GCTCTCTGGCTAACTAGAG**

Table 5 | **Q5 PCR planer set up for barcode plate master mixes.**

Detailed workflow for preparation of Q5-based barcode PCR master mixes across three mutant batches. The table lists PCR plate names, Milli-Q water, Q5 Reaction Buffer, DNA, primer combinations, universal forward primer, barcoded reverse primers, Q5 High GC Enhancer, dNTPs, and Q5 High-Fidelity DNA Polymerase exact volumes used for systematic plate setup.

Q5 PCR PLANNER				1	2	3	4a	4b	5	6	7
PCR Name	**DNA name**	**Primer name MIX**	**Total volume (µl)**	**Water**	**Buffer volume (µl)**	**DNA volume (µl)**	**Primer 1 (PBJ_Fwd_Uni) volume (µl)**	**Primer 2 (PBJ1, PBJ2 or PBJ3) volume**	**Q5 Enhancer volume (µl)**	**dNTPs volume (µl)**	**Q5 Polymerase volume (µl)**
FNV-ONT1	BC1-1	PBJUNI + PBJ1	25	12.25	5	1	1	1	2.5	2	0.25
FNV-ONT2	BC2-1	PBJUNI + PBJ1	25	12.25	5	1	1	1	2.5	2	0.25
FNV-ONT3	BC3-1	PBJUNI + PBJ1	25	12.25	5	1	1	1	2.5	2	0.25
FNV-ONT4	BC4-1	PBJUNI + PBJ1	25	12.25	5	1	1	1	2.5	2	0.25
FNV-ONT5	BC5-1	PBJUNI + PBJ1	25	12.25	5	1	1	1	2.5	2	0.25
Barcode 1 Master Mix			125	61.25	25	0	5	5	12.5	10	1.25
PCR Name	**DNA name**	**Primer name MIX**	**Total volume (µl)**	**Water**	**Buffer volume (µl)**	**DNA volume (µl)**	**Primer 1 (PBJ_Fwd_Uni) volume (µl)**	**Primer 2 (PBJ1, PBJ2 or PBJ3) volume**	**Q5 Enhancer volume (µl)**	**dNTPs volume (µl)**	**Q5 Polymerase volume (µl)**
FNV-ONT6	BC1-2	PBJUNI + PBJ2	25	12.25	5	1	1	1	2.5	2	0.25
FNV-ONT7	BC2-2	PBJUNI + PBJ2	25	12.25	5	1	1	1	2.5	2	0.25
FNV-ONT8	BC3-2	PBJUNI + PBJ2	25	12.25	5	1	1	1	2.5	2	0.25
FNV-ONT9	BC4-2	PBJUNI + PBJ2	25	12.25	5	1	1	1	2.5	2	0.25
FNV-ONT10	BC5-2	PBJUNI + PBJ2	25	12.25	5	1	1	1	2.5	2	0.25
Barcode 1 Master Mix			125	61.25	25	0	5	5	12.5	10	1.25
PCR Name	**DNA name**	**Primer name MIX**	**Total volume (µl)**	**Water**	**Buffer volume (µl)**	**DNA volume (µl)**	**Primer 1 (PBJ_Fwd_Uni) volume (µl)**	**Primer 2 (PBJ1, PBJ2 or PBJ3) volume (µl)**	**Q5 Enhancer volume (µl)**	**dNTPs volume (µl)**	**Q5 Polymerase volume (µl)**
FNV-ONT11	BC1-3	PBJUNI + PBJ3	25	12.25	5	1	1	1	2.5	2	0.25
FNV-ONT12	BC2-3	PBJUNI + PBJ3	25	12.25	5	1	1	1	2.5	2	0.25
FNV-ONT13	BC3-3	PBJUNI + PBJ3	25	12.25	5	1	1	1	2.5	2	0.25
FNV-ONT14	BC4-3	PBJUNI + PBJ3	25	12.25	5	1	1	1	2.5	2	0.25
FNV-ONT15	BC5-3	PBJUNI + PBJ3	25	12.25	5	1	1	1	2.5	2	0.25
Barcode 1 Master Mix			125	61.25	25	0	5	5	12.5	10	1.25

Table 6 | **Thermocycler steps and conditions for PCR barcoding.**

Thermal cycling parameters used during PCR barcoding.

Step	Temperature (°C)	Time	Cycles
Initial denaturation	98	30 seconds	1
Denaturation	98	10 seconds	28
Aneealing	55	30 seconds	28
Extension	72	2 minutes	28
Final extension	72	7 minutes	1
Hold	12	Indefinite	-

A) Base line relative fluorescence traces

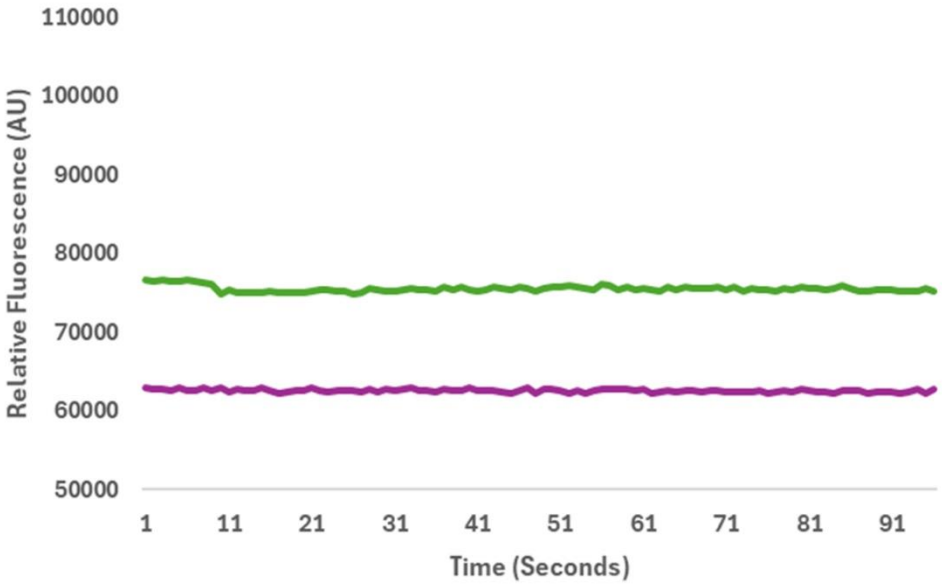

B) Relative fluorescence traces after vehicle injection

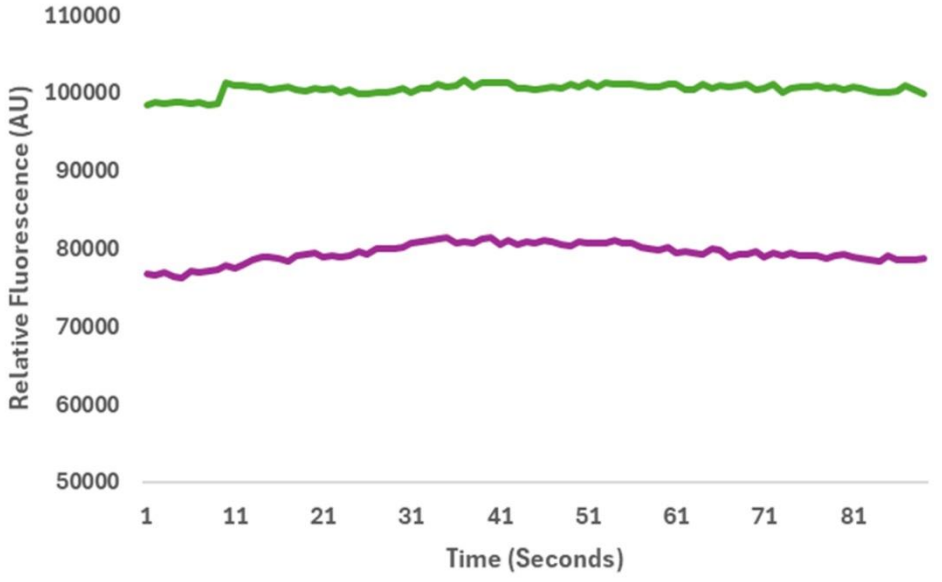

Figure 12 | **Baseline and vehicle control fluorescence traces for HEK293 cells.**

A) Relative fluorescence traces of transfected (green) and untransfected (purple) HEK293 cells over time without stimulation, showing stable baseline signals. B) Relative fluorescence traces of transfected (green) and untransfected (purple) HEK293 cells following high-volume HBSS injection, indicating minimal fluorescence changes due to vehicle addition.

A) Negative control relative fluorescence traces to AngII stimulus

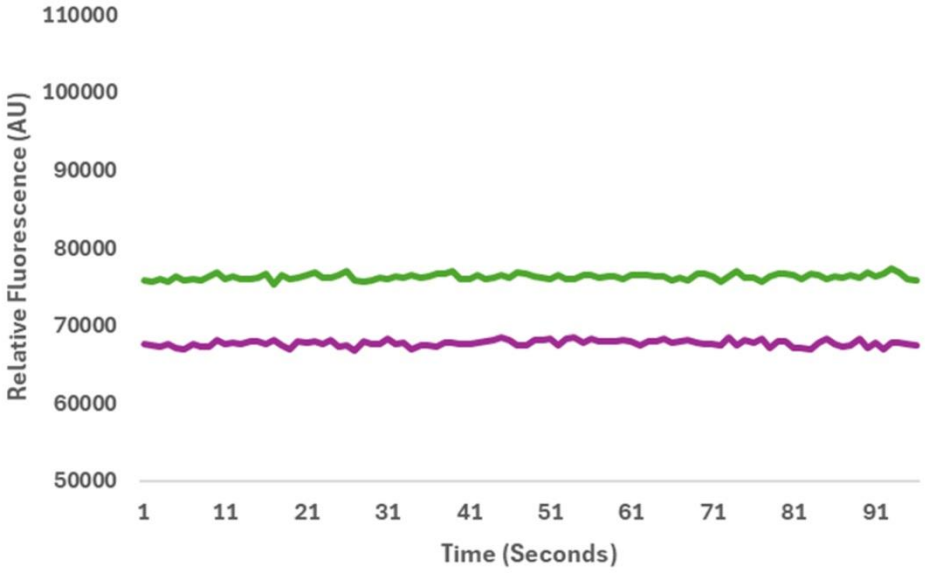

B) Relative fluorescence traces to AngII stimulus

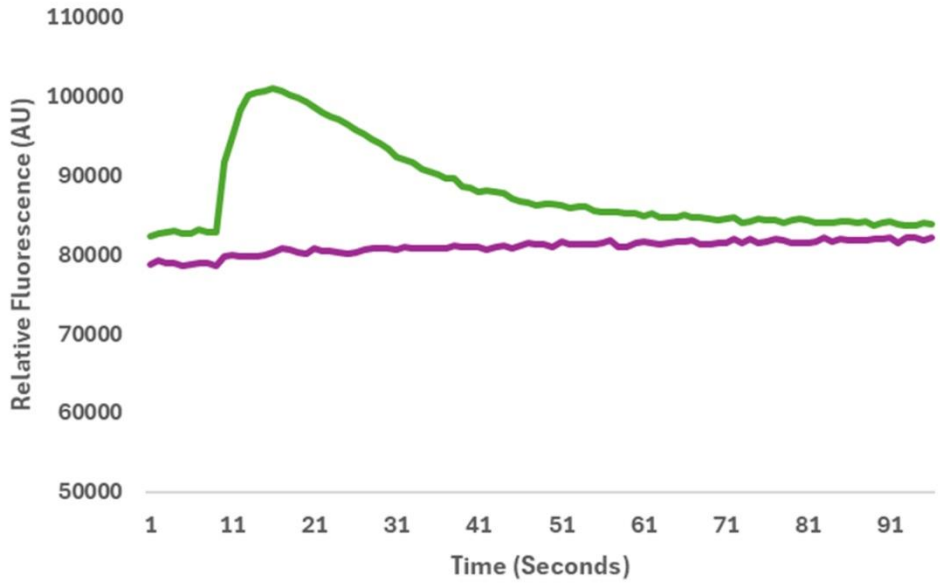

Figure 13 | **Ang II-stimulated fluorescence responses in HEK293 cells.**

A) Relative fluorescence traces of transfected (green) and untransfected (purple) HEK293 cells exposed to Ang II, showing no appreciable response in the negative control condition. B) Relative fluorescence traces of transfected (green) and untransfected (purple) HEK293 cells following AngII stimulation, showing an Ang II-dependent increase in fluorescence in transfected cells that is not observed in untransfected cells.